

1 Membrane capacitance measurements revisited: dependence of capacitance value on  
2 measurement method in non-isopotential neurons  
3

4 Jorge Golowasch<sup>1,2</sup>, Gladis Thomas<sup>3,\*</sup>, Adam Taylor<sup>4</sup>, Arif Patel<sup>1</sup>, Arlene Pineda<sup>1</sup>,  
5 Christopher Khalil<sup>1</sup>, Farzan Nadim<sup>1,2</sup>  
6

7 <sup>1</sup>Department of Mathematical Sciences, New Jersey Institute of Technology,  
8 Newark, NJ 07102

9 <sup>2</sup>Federated Department of Biological Sciences, New Jersey Institute of  
10 Technology and Rutgers University, Newark, NJ 07102

11 <sup>3</sup>Integrative Neuroscience Program, University of Medicine and Dentistry of  
12 New Jersey, Newark, NJ 07107

13 <sup>4</sup>Department of Biology and Volen Center for Complex Systems, Brandeis  
14 University, Waltham, MA 02454  
15

16 **Running title:** Capacitance measurements in non-isopotential cells  
17

18 Total # of pages: 42

19 # of Figures: 8

20 # of Tables: 1

21 # of Appendices: 1  
22

23 **Corresponding author:**

24 Jorge Golowasch  
25 New Jersey Institute of Technology  
26 Department of Mathematical Sciences  
27 323 Martin Luther King Blvd.  
28 Cullimore Hall Room 606  
29 Newark, NJ 07102

30 **Phone:** (973) 353-1267

31 **Fax:** (973) 353-5518

32 **Email:** [Jorge.P.Golowasch@njit.edu](mailto:Jorge.P.Golowasch@njit.edu)  
33

34 \* Current Address: Drexel University College of Medicine; Department of Neurobiology  
35 and Anatomy; Philadelphia, PA 19129

36 **Keywords:** capacitance, voltage-clamp, current-clamp, electrophysiology,  
37 model, methods

38 **Abstract**

39

40 During growth or degeneration neuronal surface area can change dramatically.  
41 Measurements of membrane protein concentration, as in ion channel or ionic conductance  
42 density, are often normalized by membrane capacitance, which is proportional to the  
43 surface area, to express changes independently from cell surface variations. Several  
44 electrophysiological protocols are used to measure cell capacitance, all based on the  
45 assumption of membrane isopotentiality. Yet, most neurons violate this assumption  
46 because of their complex anatomical structure, raising the question of which protocol  
47 yields measurements that are closest to the actual total membrane capacitance. We  
48 measured the capacitance of identified neurons from crab stomatogastric ganglia using  
49 three different protocols: the current clamp step, the voltage clamp step and the voltage  
50 clamp ramp protocols. We observed that the current clamp protocol produced  
51 significantly higher capacitance values than either voltage clamp protocol. Computational  
52 models of various anatomical complexities suggest that the current clamp protocol can  
53 yield accurate capacitance estimates. In contrast, the voltage clamp protocol estimates  
54 rapidly deteriorate as isopotentiality is reduced. We provide a mathematical description  
55 of these results by analyzing a simple two-compartment model neuron to facilitate an  
56 intuitive understanding of these methods. Together, the experiments, modeling and  
57 mathematical analysis indicate that accurate total membrane capacitance measurements  
58 cannot be obtained with voltage clamp protocols in non-isopotential neurons.  
59 Furthermore, although current clamp steps can theoretically yield accurate measurements,  
60 experimentalists should be aware of limitations imposed by step duration and numerical  
61 errors during fitting procedures to obtain the membrane time constant.

62

63 **Introduction**

64

65 During development, growth or neuronal degeneration, cell size can change dramatically  
66 and neuronal plasticity may involve changes in the cell surface area (Chklovskii et al.  
67 2004). Because total membrane capacitance is directly proportional to the membrane  
68 surface area, it is an important cellular feature to measure to express changes in cellular  
69 properties after taking size differences and changes into account. Changes in ionic  
70 conductance during plasticity or developmental changes, for example, are often expressed  
71 as conductance densities in order to remove potential effects of changes in neuronal size  
72 during these processes (Haedo and Golowasch 2006; Iwasaki et al. 2008; Khorkova and  
73 Golowasch 2007; Pineda et al. 2008; Royeck et al. 2008).

74

75 Several experimental methods exist for determining total membrane capacitance, which  
76 rely on neuronal membranes having a specific membrane capacitance that is similar in  
77 most cells and generally agreed to be 0.5-1.0  $\mu\text{F}/\text{cm}^2$  (Koch 1999; Solsona et al. 1998).  
78 Capacitance can be calculated from the rate and amplitude changes in the voltage or  
79 current responses under current- and voltage-clamp, respectively. These methods are used  
80 extensively to determine the total membrane capacitance of neurons of various sizes and  
81 architectures. However, these methods were derived for, and can correctly be applied  
82 only to, isopotential cells. Biological neurons rarely conform to this constraint.  
83 Consequently, these methods are likely to yield incorrect estimates of cell capacitance  
84 and consequently cell surface area. Nevertheless, a cursory look at current editions of  
85 major neuroscience journals indicates that capacitance measurements are made without  
86 regard to the validity of the assumptions underlying the method employed. Assessing the  
87 accuracy of these methods to estimate total membrane capacitance in neurons with  
88 complex architectures is essential if capacitance measurements are to be used to make  
89 correct inferences about changes in cell surface area as a measure of neuronal  
90 conductance density changes.

91

92 We compared the capacitance values of identified neurons in the crab stomatogastric  
93 nervous system using three of the most commonly used methods for capacitance

94 measurement. We show that these different protocols yield significantly different values  
95 for the measured total membrane capacitance in the same neuron. We then evaluate the  
96 accuracy of these methods using simple computer models of non-isopotential cells. Our  
97 results confirm that appropriate exponential fits to voltage profiles in response to DC  
98 current step injection can provide an accurate measure of total membrane capacitance  
99 values over a wide range of cell sizes and architectures (see Major et al., (1993a) for a  
100 theoretical analysis). In contrast, measurements of the charge accumulated in the  
101 membrane capacitor using voltage-clamp steps, which are among the most commonly  
102 used method in electrophysiology (cf. (Haedo and Golowasch 2006; Iwasaki et al. 2008;  
103 Khorkova and Golowasch 2007; Pineda et al. 2008; Royeck et al. 2008) yields the least  
104 accurate capacitance estimates. To provide insight into the discrepancy observed in these  
105 methods, we use a simple two-compartment model to derive mathematical expressions  
106 that show the source of the different total membrane capacitance measurements with the  
107 current- and voltage-clamp protocols. Equivalent equations can also be derived in more  
108 general form, for an arbitrary tree-like neuronal structure, from the theoretical work of  
109 Major et al., (1993a, b). Our results suggest that, while current-clamp steps should be the  
110 preferred method to reduce the inaccuracies in capacitance determination, the difference  
111 in capacitance values measured with the different methods can be used to make  
112 approximate inferences about cell surface distribution among different neuronal  
113 compartments. A simple two-compartment theoretical analysis can be used to obtain an  
114 intuitive understanding of the source of errors in total capacitance measurement with  
115 these different methods.  
116

117 **Methods**

118

119 *Electrophysiology*

120 The lateral pyloric (LP) and pyloric dilator (PD) neurons from the pyloric network of the  
121 crab *Cancer borealis*, localized in the stomatogastric ganglion (STG), were identified  
122 using standard procedures previously described (Harris-Warrick 1992; Selverston et al.  
123 1976). Individual neurons were then impaled with two microelectrodes pulled using a  
124 Flaming-Brown micropipette puller (P87, Sutter Instruments, CA) and filled with a 0.6 M  
125  $K_2SO_4 + 20$  mM KCl solution (electrode resistance was 20-25 M $\Omega$ ). One of the  
126 electrodes was used to pass current and the other to record voltage. Neurons were  
127 recorded in either two-electrode current clamp or two-electrode voltage clamp mode  
128 using an Axoclamp 2B amplifier (Molecular Devices, Union City, CA). In voltage clamp  
129 mode, the amplifier gain was set to a value around 3-8. We did not attempt to increase the  
130 gain to its maximum possible even if stability could be ensured using appropriate phase  
131 lag settings (see below). The preparations were bathed in 10  $\mu$ M picrotoxin (Sigma-  
132 Aldrich, St. Louis, MO) to block glutamatergic synaptic input, 0.1  $\mu$ M tetrodotoxin  
133 (TTX; Biotium, Hayward, CA) to block fast  $Na^+$  current-dependent action potentials and  
134 consequently all oscillatory activity, and 5 mM CsCl to block the hyperpolarization-  
135 activated inward current. Capacitance was measured at voltages between -50 and -60  
136 mV to avoid activation of voltage-gated currents (Golowasch and Marder 1992; Haedo  
137 and Golowasch 2006). Data were acquired with the Digidata 1322A board and pClamp  
138 9.2 software (Molecular Devices, Union City, CA).

139

140 *Capacitance measurements*

141 1) *Current clamp protocol (CC\_step)*. DC current steps (-0.5 to -2 nA, 500-1000 msec  
142 duration) were injected in the soma and the membrane potential ( $V_m$ ) change was  
143 recorded with a sampling rate of 50 kHz. 30 consecutive traces were averaged to remove  
144 noise. In an isopotential cell this results in a membrane potential change characterized by  
145 a single exponential (Eq. 1) with time constant  $\tau_m = r_m c_m$  where  $r_m$  is the cell membrane  
146 resistance and  $c_m$  the total membrane capacitance. In such an isopotential cell,  $r_m$  is equal  
147 to the cell's input resistance  $R_{in}$ . The maximal membrane potential change is given by

148  $\Delta V_m = V_m - V_{rest} = R_{in} I_{ext}$ , where  $I_{ext}$  is the injected current step. When a cell is non-  
 149 isopotential, an equalizing process related to current flow between electrical  
 150 compartments of the cell takes place (Major et al. 1993a; Rall 1977), the membrane  
 151 potential change  $\Delta V_m(t)$  is now determined by a series of exponential terms (Eq. 1), and  
 152  $R_{in}$  is no longer equal to  $r_m$ . Typically only two or three terms adequately describe  $V_m(t)$   
 153 (Fig. 1A):

$$154$$

$$155 \quad V_m(t) = V_{rest} + \sum_{i=0}^{\infty} V_i (1 - e^{-t/\tau_i}) \quad (1)$$

156  
 157 By dividing through by  $I_{ext}$ , one obtains a series of resistive terms  $R_i = V_i / I_{ext}$ . At steady  
 158 state, the sum of these resistive terms is  $R_{in} = \Delta V_m / I_{ext}$ . The time constant of the slowest  
 159 exponential term  $\tau_0$  corresponds to the membrane time constant  $\tau_m = r_m c_m$  (Holmes et al.  
 160 1992; Major et al. 1993a; Rall 1977). To determine the values of  $V_i$  and  $\tau_i$  we fit the  $V_m(t)$   
 161 curve obtained in response to the current step using two or three exponential terms using  
 162 the Levenberg-Marquardt (LM) algorithm of the Clampfit analysis software in the  
 163 pClamp package with a precision of  $10^{-6}$ . In order to obtain the best fits to both fast and  
 164 slow components, we fit the trace between  $t = 0$  and a time at which the voltage had  
 165 reached steady state, usually the end of the 500-1000 msec step.

166  
 167 2) *Voltage clamp step protocol (VC\_step)*. Steps 1000 msec long between  $-50$  and  
 168  $-60$  mV were applied in voltage clamp and 20-30 sweeps were averaged to remove noise.  
 169 The membrane current and membrane potential were sampled at 50 kHz. This method  
 170 relies on the measurement of the total charge  $Q$  accumulated on the membrane capacitor  
 171 during the initial (capacitive) current transient (Fig. 1B, gray area) and can be calculated  
 172 with Equations 2, 3:

$$173$$

$$174 \quad Q = c_m \Delta V_m \quad (2)$$

$$175 \quad Q = \int_0^{t_p} I_c dt \quad (3)$$

176  
 177 where  $t_p$  is the step duration.

178

179 The determination of the capacitive transient's integral is sensitive to the rate of current  
180 change during the transient. This sensitivity is due to aliasing if the sampling frequencies  
181 are lower than the Nyquist frequency (Harris 2006). In turn, the rate of current change  
182 increases with the gain setting of the voltage clamp. Thus, the voltage clamp gain was set  
183 high enough to ensure that the voltage settled at the test voltage within the duration of the  
184 step, but not necessarily at the highest possible value to avoid aliasing.

185

186 3) *Voltage clamp ramp protocol (VC\_ramp)*. Ramps of voltage were applied from a  
187 holding membrane potential of  $-50$  mV. A  $10$  mV hyperpolarizing ramp was  
188 immediately followed by a  $10$  mV depolarizing ramp of the same duration (Fig. 1C, left  
189 panel, top trace). The protocol was repeated  $30$  times and the current traces were  
190 averaged to remove noise (Fig. 1C, left panel, bottom trace). Two different ramp slopes  
191 were used:  $0.02$  and  $0.5$  mV/msec. The sampling rate was set to  $50$  kHz and the same  
192 gain setting as in the voltage clamp step protocol was used. The current was plotted  
193 versus the voltage (Fig 1C, right panel) and the capacitive current was obtained by  
194 measuring the resulting capacitive current difference ( $2i_c$ ) between the two ramps at a  
195 given voltage. We used the average current values around the middle  $50\%$  of the I-V  
196 curve to measure  $2i_c$  avoiding the beginning and end of the ramps to avoid spurious  
197 effects (Fig 1C, grey area in the right panel).  $c_m$  was calculated according to:

198

$$199 \quad i_c = \frac{dQ}{dt} = c_m \frac{dV_m}{dt} \quad (4)$$

200

201 where  $\frac{dV_m}{dt}$  corresponds to the slope of the voltage ramp (Fig. 1C, top left trace).

202

### 203 *Modeling*

204

205 We used model anatomical structures of varying complexity, with the simplest consisting  
206 of two spheres attached to the respective ends of a cable, which represents a neurite, and

207 has length  $len$  and diameter  $d_c$ . One sphere represents the soma (with diameter  $d_s$ ), and  
 208 current and voltage are measured and manipulated only in this compartment. The second  
 209 sphere represents the combined area of all dendrites and has diameter  $d_d$ . We modeled  
 210 variations in neuronal size by changing  $d_d$  (see inset in Fig. 3A). More complex models  
 211 are tree-like structures with a sphere (the soma) attached to a cable (the primary neurite)  
 212 and additional branched cables, representing dendrites of various orders, attached to the  
 213 opposite end. In the “asymmetric tree” structure, the second, third and fourth order  
 214 neurites are connected to only one branch of the primary or n-1 order neurites (see inset  
 215 in Fig. 5A). The number of primary dendrites was limited to two, secondary dendrites to  
 216 four and tertiary dendrites to eight, and each higher order dendrite had a diameter of 1/2  
 217 of the previous order dendrite diameter. A “concentric” tree was built by attaching all  
 218 these higher order dendrites directly to the soma (see inset in Fig. 5B), and a “symmetric  
 219 tree” was built by distributing the same number of dendrites symmetrically, i.e. instead of  
 220 all secondary and tertiary branches always originating respectively in the same primary  
 221 and secondary dendrite, they are distributed evenly among all the n-1 order dendrites (see  
 222 inset in Fig. 5C).

223

224 Passive cables and spheres were used for these models and the passive parameters were  
 225 chosen as  $C_m = 1\mu\text{F}/\text{cm}^2$ ,  $R_m = 40,000\ \Omega\text{cm}^2$ ,  $R_a = 60\ \Omega\text{cm}$  (Rabbah et al. 2005). For  
 226 simulations, each cable was compartmentalized into segments with length of at most  
 227  $\lambda/20$ , and each compartment  $j$  obeyed the current balance equation:

228

$$229 \quad c_{m_j} \frac{dV_{m_j}}{dt} = I_{ext} - (I_{leak,j} + I_{axial,j}) \quad (5)$$

230

231 Where  $I_{leak,j}$  is the linear leak current of compartment  $j$  and  $I_{axial,j}$  is the axial current  
 232 flowing from adjacent compartment(s) into compartment  $j$ .

233

234 The membrane and cable equations were numerically integrated using the software  
 235 Network (<http://stg.rutgers.edu/software/network.htm>) using a fourth-order Runge-Kutta

236 integration method and a time step of 10  $\mu$ s. Simulation data were sampled at 10 KHz for  
237 the CC\_step and VC\_ramp protocols and at 100 KHz for the VC\_step protocol.  
238

239 **Results**

240

241 *Measurement protocol determines capacitance measurement discrepancies*

242 We explored how the measured capacitance of a neuron depends on the particular  
243 protocol used by examining measured values with distinct protocols in the crab pyloric  
244 dilator (PD) and lateral pyloric (LP) neurons, which are readily identified in the STG.  
245 Three measurement protocols were used, one using current steps and the other two in  
246 voltage clamp mode (see Methods).

247

248 Measurements of capacitance using DC current steps depend on accurate measurement of  
249 the membrane time constant and resistance. Frequently, when this method is used to  
250 estimate the total membrane capacitance of a neuron,  $c_m$  is derived by dividing  $\tau_m$  by the  
251 input resistance  $R_{in}$  (e.g. (Dougherty et al. 2005; Golowasch and Marder 1992). While  
252 this is correct for an isopotential cell, in which case  $V_m(t)$  can be fit with a single  
253 exponential term, it is not correct for a non-isopotential cell. In the case of a finite tree  
254 with sealed ends,  $V_m(t)$  can be fit as a sum of exponentially decaying terms given by  
255 Equation 1, where  $\tau_0 > \tau_1 > \tau_2 > \dots$  is a sequence of time constants (Major et al. 1993a;  
256 Rall 1977). The slowest component corresponds to the charging of the membrane  
257 capacitor and therefore the exponential fit to the slowest component provides the  
258 membrane time constant  $\tau_m$ . The correct measurement of  $c_m$  is obtained by dividing  $\tau_m$  (=  $\tau_0$ )  
259 by the resistance coefficient  $R_0 = V_0/I_{ext}$  (and not the input resistance of the cell)  
260 (Major et al. 1993a). In practice, the passive response of a neuron to DC current injection  
261 can be adequately fit with only two or three exponential terms. The diagram in Fig. 1A  
262 shows the membrane potential response ( $V_m$ , dark trace) to a current step ( $I_{ext}$ ). In the case  
263 shown,  $V_m$  can be decomposed into two exponentially decaying components whose sum  
264 adequately fits this voltage trace (grey traces). Once again, the correct measurement of  $c_m$   
265 in this case is obtained as  $\tau_0/R_0$ . To demonstrate the difference in the measured values  
266 when using  $R_{in}$  or  $R_0$ , we compared these measurements in recordings of PD neurons. The  
267 time constant is  $151.10 \pm 89.52$  msec (N = 29). The calculated  $c_m$  using  $R_{in}$  was  $12.43 \pm$   
268  $7.44$  nF whereas, using  $R_0$ , the value was  $65.61 \pm 68.63$  nF (Student t-test, P < 0.0001, N

269 = 29). It is these latter values that we use as our measurements for CC\_step in both the  
270 experimental protocols and in the computational models described below in the Results.

271

272 We compared the CC\_step measurements with measurements done using the voltage  
273 clamp step (VC\_step) protocol and the voltage clamp ramp (VC\_ramp) protocol using  
274 two different slopes of 0.02 and 0.5 mV/msec (Fig. 2). In measurements from either the  
275 PD neuron or the LP neuron, these values were significantly different (Kruskal-Wallis  
276 One-way ANOVA on Ranks,  $P < 0.0001$ , for both PD and LP neurons, see Table 1, Fig.  
277 2). A post-hoc analysis using the Dunn's Method showed that the current clamp estimate  
278 of capacitance is significantly higher than either of the two voltage clamp methods, and  
279 that the fast voltage clamp ramp method is significantly different from either VC\_step or  
280 slow (0.02 mV/msec) voltage clamp ramp method.

281

282 To explore the source of this large difference in total membrane capacitance estimates  
283 obtained using the current clamp and voltage clamp protocols, we built a simple passive  
284 model and measured its total membrane capacitance using these three protocols. The  
285 model consisted of a spherical soma of fixed diameter connected to a cable representing a  
286 primary neurite connecting the soma to more distal compartments (see Methods for  
287 parameters). The distal end of the cable was connected to a second sphere representing  
288 the equivalent area of distant dendritic compartments (Fig. 3A). With the exception of the  
289 length of the neurite, the passive membrane parameters used are approximations to values  
290 assumed to be typical of PD neurons until now (Nadim and Golowasch 2006; Rabbah et  
291 al. 2005); (Hartline and Castelfranco 2003). With these parameters, the dendritic  
292 compartment is at an electrotonic distance of  $L = len/\lambda = 0.25$  away from the soma.

293 Figure 3B shows the results of applying the current clamp and voltage clamp protocols by  
294 recording the voltage and injecting current into the soma compartment and varying the  
295 diameter of the dendritic "sphere."

296

297 The capacitance values measured in the model cell were normalized to their actual  
298 capacitance (determined from the total cell surface and the specific membrane  
299 capacitance  $C_m$ ) and are shown in Fig. 3B as colored circles. The current clamp protocol

300 yielded capacitance estimates (using the  $\tau_m / R_0$  measurement described above) that were  
301 indistinguishable from the actual capacitance of the cell for all values of dendritic  
302 compartment size tested (black symbols). However, capacitance value measurements  
303 obtained with the voltage clamp protocols underestimated actual capacitance values for  
304 all dendritic compartment sizes, with errors increasing rapidly as the dendritic  
305 compartment diameter exceeded  $\sim 100 \mu\text{m}$ . Estimates obtained with the ramp protocol  
306 depended on the slope of the voltage ramp ( $dV/dt$ ), with better results obtained with the  
307 slow ramps ( $dV/dt = 0.02 \text{ mV/msec}$ , green circles). Faster ramps (blue circles) led to  
308 increasingly worse capacitance estimates than those obtained with the voltage clamp step  
309 protocol (red circles). Voltage ramps with slopes lower than  $0.02 \text{ mV/msec}$  did not  
310 improve the capacitance estimates significantly and are not shown. Reducing the pulse  
311 duration in the VC\_step protocol further reduced the capacitance estimates. Adding noise  
312 to the voltage traces obtained with the current clamp protocol had a minimal impact on  
313 the capacitance estimates ( $<1\%$  error with  $5 \text{ kHz}$  white noise current injection of  $5\%$   
314 amplitude as the current step; not shown).

315

316 To determine if such a simple model could represent the surface distribution of a  
317 biological neuron, we compared the capacitance values of the biological PD and LP  
318 neurons measured with the three protocols (and two different voltage ramp slope values)  
319 with the values obtained in the model. The biological capacitance values obtained are  
320 listed in Table 1, and the normalized values (normalized to each neuron's capacitance  
321 value measured with the CC\_step protocol) are plotted in Figure 3B (LP neuron: squares,  
322 PD neuron: stars). When these data were compared to the data obtained with the same  
323 protocols on the ball-stick-ball model we found that the PD neuron could reasonably be  
324 fit by a model with an approximate dendritic "sphere" diameter  $d_d$  of  $820 \mu\text{m}$ , and the LP  
325 neuron with an approximate diameter  $d_d$  of  $700 \mu\text{m}$ . The comparison derived from Fig.  
326 3B is only meaningful in two general ways: it indicates that the "dendritic compartment"  
327 is much larger than the "somatic compartment" in both neuron types, and it suggests that  
328 PD neurons appear to have a larger dendritic surface area than LP neurons.

329

330 Because the voltage clamp step and ramp protocols (with  $dV/dt = 0.02$  mV/msec) yielded  
331 similar results henceforth we only show the VC\_step data

332

333 *Effect of membrane leak, resistivity and electrotonic length on capacitance measurement*

334 Using our simple ball-stick-ball model we examined the effect of three important factors  
335 that are commonly thought to affect current and voltage clamp measurements: soma leak  
336 (such as is induced by the damage to the membrane due to microelectrode penetration),  
337 overall membrane resistivity, and the electrotonic distance of the distal dendritic  
338 compartment from the soma. Changes in the conductance of the soma compartment alone  
339 (range: 0.5-125 nS) had no effect at all on the total membrane capacitance when  
340 measured with either voltage clamp protocol, but greatly affected the measurement using  
341 the current clamp protocol. In Figure 3C, the effect of changing the soma conductance on  
342 capacitance measurement is plotted as a function of the resulting input resistance  $R_{in}$  in  
343 each case. High values of soma resistance tended to lead to slight underestimates of the  
344 total membrane capacitance with the CC\_step protocol whereas low soma resistance led  
345 to marked overestimates (Fig. 3C). In contrast, reducing the specific membrane resistivity  
346  $R_m$  uniformly over the entire surface of the cell markedly reduced the estimates obtained  
347 with both voltage clamp protocols (Fig. 3D), but had little impact on the estimates  
348 obtained with the CC\_step protocol.

349

350 The membrane voltage attenuates with the distance from the point of current injection.  
351 Therefore, the electrotonic distance of the dendritic compartment from the point of  
352 measurement (i.e. the soma) is likely to affect the accuracy of the capacitance  
353 measurements. To determine how the  $c_m$  value obtained by different measurement  
354 protocols may be affected by the electrotonic size of the neuron, we used the same model  
355 and varied the length of the neurite while keeping the dendrite diameter fixed (Fig. 4A).  
356 Capacitance estimates using the current clamp protocol yielded almost perfect estimates  
357 for up to approximately 1 length constant away from the soma even for the largest  
358 dendritic compartment (i.e.  $d_d = 1000$   $\mu\text{m}$ , Fig. 4B). For electrotonic lengths  $L > 1$ , the  
359 capacitance measurement deteriorated in a manner that depends on the dendrite  
360 compartment size. The capacitance measurement error is nevertheless remarkably small

361 even with a dendrite diameter of  $d_d = 200 \mu\text{m}$  (Fig. 4B) and almost nonexistent when no  
362 dendrite compartment is added, i.e.  $d_d = 0 \mu\text{m}$  (Fig. 4B). When the voltage clamp step  
363 protocol is used, these estimates drop much more abruptly. In this case, error values of  $<$   
364 20% are obtained for  $L < 0.75$  when no dendritic compartment is present or  $L < 0.15$  with  
365 a dendrite with diameter  $200 \mu\text{m}$  (Fig. 4C). For all other conditions the errors are much  
366 larger and, for  $L > 1.4$ , the voltage clamp protocol results in errors of  $> 50\%$  even when  
367 no dendritic compartment exists.

368

### 369 *Effect of neuronal architecture on capacitance measurements*

370 Since both the size of the dendritic compartment and its distance from the site of  
371 measurement affect all of the capacitance estimates, we built more complex and realistic  
372 neuronal models to better understand the role of neuronal architecture on capacitance  
373 measurements. Figure 5 shows capacitance measurements in three different neuronal  
374 models. The first of these models (“asymmetric tree”, see diagram in Fig. 5A) consists of  
375 a soma connected to a tree of branching dendrites, all with equal length ( $len = 1000 \mu\text{m}$ ;  
376 see Methods for additional parameters). Each dendritic “level” has one-half the diameter  
377 and at most double the number of branches of the previous level. All branches in a given  
378 level emerge from only one of the branches from the previous level (see diagram in Fig.  
379 5A, *inset*). The first (primary) dendritic level consisted of a single cable with diameter  $d_{c1}$   
380  $= 9.6 \mu\text{m}$ , which was connected to either one or two secondary dendrites with diameter  
381  $d_{c2} = 4.8 \mu\text{m}$ , and so on.

382

383 In order to examine the effect of the complexity of the tree architecture we added one  
384 branch at a time and measured capacitance of the cell with the three methods described  
385 above. With this architecture, when all branches are present (i.e. each dendritic level has  
386 exactly double the number of branches of the preceding branch), the total capacitance of  
387 each dendritic level is the same. Again, as with the simpler model, we observed that the  
388 current clamp protocol (Fig. 5A, filled symbols) yields capacitance values that are much  
389 closer to the actual total capacitance (identity line) than the voltage clamp protocols (Fig.  
390 5A, open symbols). The two clusters that can be observed with the VC\_step data are due  
391 to the presence of either one (lower cluster) or two (higher cluster) secondary level

392 branches, because an additional secondary branch adds a large amount of capacitance at a  
393 short electrotonic distance from the soma. The same phenomenon occurs when the  
394 CC\_step method is used, except that the data are closer to the identity line, making it  
395 more difficult to distinguish the clusters. The apparent “branches” emerging from the  
396 identity line for the CC\_step protocol data correspond to changes in tertiary branch  
397 numbers, with the values along each branch corresponding to variation in quaternary  
398 branch numbers. The abrupt decreases in capacitance when new branches are added are  
399 probably due to increasingly large numerical errors in the multi-exponential fitting  
400 procedure, since it has been shown that the slow exponential term correctly represents the  
401 charging of the membrane in neurons of any arbitrarily complex architecture (Major et al.  
402 1993a). The same phenomenon is also observed with the VC\_step data but here the data  
403 corresponding to tertiary branch numbers are less clearly separated. As in the simpler  
404 model, voltage clamp ramp protocol results (with  $dV/dt = 0.02$  mV/msec) were very  
405 similar to those obtained with the voltage clamp step protocol and are not shown.

406

407 In order to examine the effect of the tree structure on these measurements, we applied the  
408 same measurements to a model neuron in which the same branches were all connected  
409 directly to the soma (“concentric tree”; see diagram in Fig. 5B). In this case all current  
410 clamp data fell almost perfectly on the identity line and the voltage clamp data deviated  
411 from this line only modestly (Fig. 5B). Thus, not surprisingly, a more compact neuronal  
412 structure yields far better capacitance estimates regardless of the number of branches,  
413 with the current clamp step method always producing values that are more accurate than  
414 either voltage clamp method (ramp data not shown).

415

416 We also explored the effect of asymmetry in the neuronal tree structure on our  
417 measurements in a symmetric model. The “symmetric tree” model was built by having  
418 the branches emerge symmetrically from the previous level dendrite, rather than having  
419 all emerge from a single dendrite (see diagram in Fig. 5C). The resulting capacitance  
420 measurements of the symmetric tree structures are plotted together with the  
421 corresponding asymmetric tree data (with the same branch numbers at each level) in Fig.  
422 5C. The number of points in this plot is lower than in Fig. 5B because there are fewer

423 possible symmetric than asymmetric structures and we plotted only those points of the  
424 asymmetric tree for which a distinct capacitance value was measured. We observe that  
425 evenly distributing the dendritic load among branches (as in the symmetric structure)  
426 improves the capacitance estimates but the differences are slight and are noticeable only  
427 for the largest tree structures.

428

429 The symmetric tree model was used to examine the effect of an axon emerging at  
430 different locations in a neuron. Figure 6A shows the effects of attaching axons of  
431 different lengths to the end of the secondary dendrite, approximately corresponding to  
432 what is observed in STG neurons (Bucher et al. 2007). Capacitance measurements  
433 obtained with the CC\_step protocol produced accurate estimates for axon lengths of  
434 several millimeters, beyond which estimates began to deteriorate. In contrast to the  
435 CC\_step measurements, VC\_step estimates rapidly deteriorated for all axon lengths. In  
436 contrast, when the axon emerges directly from the cell body, as is commonly seen in  
437 vertebrate CNS neurons, CC\_step total capacitance estimates are accurate for much  
438 longer axons than in the previous case.

439

440 Finally, in order to evaluate the degree to which neuronal complexity affects the  
441 determination of cell capacitance, we calculated a complexity index for the tree structures  
442 based on the electrotonic length of each dendrite. The complexity index was defined  
443 simply as the sum of the electrotonic lengths of all dendrites of the cell. Figure 7 shows  
444 the same data as in Fig.5A, B, indicating again that the current clamp method provides a  
445 good estimate of cell capacitance for the neurons with fewer branches, i.e. lowest  
446 complexity index (Fig. 7A, filled symbols). However, some estimates have large errors  
447 even when the complexity index is low. Closer inspection of the data reveals that in all  
448 such cases the cells had a high number of quaternary dendrites ( $>5$ ), but low number of  
449 lower level dendrites. This generated low complexity index values but a widely  
450 distributed capacitance, which in turn leads to large capacitance estimate errors. In  
451 general, however, there is a relatively good correlation of the measurement error level  
452 and neuronal complexity (i.e. branch number and total electrotonic length). The voltage  
453 clamp protocol produces much larger estimate errors (Fig. 7A, open symbols), with two

454 distinct clusters due to the presence of either two (high error level cluster) or only one  
455 (low error level cluster) secondary level branches (also seen in Fig. 5A). The concentric  
456 cell in which all branches emerge directly from the soma predictably produces much  
457 lower estimate errors with both current and voltage clamp methods, as would be expected  
458 from an electrotonically more compact neuron, with voltage clamp protocols again  
459 generating many-fold larger errors than the current clamp protocol (Fig. 7B).

460

461 *The discrepancy between the voltage clamp and the current clamp measurements can be*  
462 *elucidated using a two-compartment model*

463 The responses to current- and voltage-clamp pulses have been previously derived for an  
464 arbitrarily complex neuronal architecture (Major et al. 1993a; b). Although the  
465 derivations of Major and collaborators can be used to estimate the effect of the methods  
466 of capacitance measurements for complex structures (particularly for the current clamp  
467 case; see Eq. 36 in (Major et al. 1993a), we present a comparison using a two-  
468 compartment model to help gain a simpler and more intuitive understanding of the factors  
469 that affect total membrane capacitance measurements in electrophysiological  
470 experiments. For brevity, we will only compare the CC\_step and VC\_step methods here,  
471 but the VC\_ramp method can be dealt with in a similar fashion, as shown in the  
472 Appendix (Eqs. A26-A31).

473

474 It can be shown that this circuit responds to a current-clamp step of size  $I_{ext}$  with a  
475 double-exponential voltage trace described by

476

$$477 \quad V_m(t) = V_{rest} + I_{ext} R_0 (1 - e^{-t/\tau_0}) + I_{ext} R_1 (1 - e^{-t/\tau_1}) \quad (8)$$

478

479 where  $R_0$ ,  $\tau_0$ ,  $R_1$ , and  $\tau_1$  ( $\tau_0 > \tau_1$ ) are constants that are determined by the values of  $R_a$  (the  
480 axial resistance) and  $C_n$ ,  $R_n$ ,  $C_f$ , and  $R_f$ , denoting, respectively, the membrane capacitance  
481 and resistance of the “near” and “far” compartments. If we assume that  $R_n C_n = R_f C_f$ , as  
482 would be the case for a cell with uniform specific membrane resistance and capacitance,  
483 then it can be shown that

484

485  $\frac{\tau_0}{R_0} = C_n + C_f$  (9)

486

487 Thus, in this simplified model, it can be proven mathematically that the current-clamp  
 488 step method described above always gives the correct answer for the total capacitance  
 489 (see Appendix).

490

491 The response of this simple model to a voltage-clamp step of size  $\Delta V_m$  can also be  
 492 derived, and is given by

493  $I(t) = \Delta V_m \cdot \left[ C_{pulse} \delta(t) + G_{in} u(t) + G_{decay} u(t) \exp\left(-\frac{t}{\tau_{vc}}\right) \right]$  (10)

494

495 where  $C_{pulse}$ ,  $G_{in}$ ,  $G_{decay}$ , and  $\tau_{vc}$  are constants determined by the values of  $R_a$ ,  $C_n$ ,  $R_n$ ,  $C_f$ ,  
 496 and  $R_f$  (see Eqs. A18-21 in the Appendix).  $\delta(t)$  is the Dirac delta function, here  
 497 representing the mathematical idealization of a large brief pulse of current corresponding  
 498 to the capacitive transient, and  $u(t)$  is the unitary step function denoting the current pulse.  
 499 If we subtract off the steady-state current and integrate, we find that the charge delivered  
 500 by the capacitive transient and the subsequent exponential decay is given by

501  $Q = \Delta V_m (C_{pulse} + G_{decay} \tau_{vc})$ . Since the voltage-clamp step estimate of capacitance is given  
 502 by  $Q/\Delta V_m$  (Eq. 2), this yields an estimate of  $C_{pulse} + G_{decay} \tau_{vc}$ . It can be shown that this  
 503 expression is equal to

504

505  $C_n + C_f \frac{1}{(1 + R_a/R_f)^2}$  (11)

506

507 (see Appendix). The factor  $1/(1 + R_a/R_f)^2$  is less than one for non-zero  $R_a$ , indicating that  
 508 the voltage-clamp method provides an underestimate of the total capacitance for all non-  
 509 isopotential cells and that this estimate approaches the capacitance of the near  
 510 compartment as the axial resistance increases.

511

512 The ratio of the VC\_step estimate of capacitance to the CC\_step estimate can be  
513 predicted from the parameters  $R_\theta$ ,  $R_l$ ,  $\tau_\theta$  and  $\tau_l$  obtained from exponential fits to voltage  
514 traces obtained with the CC\_step protocol (Eq. A26 in Appendix). This is demonstrated  
515 in Fig. 8B where the normalized total membrane capacitance is plotted as a function of  
516 the dendritic compartment diameter in our simple ball-stick-ball model neuron, for  
517 capacitance values determined with the VC\_step protocol (same data as in Fig. 3B) and  
518 applying Eq. A26 to parameters measured with the CC\_step protocol. The same is not  
519 true when the neuronal anatomy is more complex and is better approximated with three  
520 or more compartments (and thus the data from CC\_step experiments are better fitted with  
521 three or more exponential terms), such as in the case of our tree-like neuron models (Fig.  
522 5) or the biological STG neurons. In these cases estimates obtained with Eq. A26 do not  
523 provide a good match to the VC\_step measurements (not shown).  
524

525 **Discussion**

526

527 Total membrane capacitance is a common measure of cell surface area and is used in  
528 electrophysiology recordings as a means for measuring ionic conductance, or ion  
529 channel, density or to normalize for changes in cell size (Haedo and Golowasch 2006;  
530 Iwasaki et al. 2008; Khorkova and Golowasch 2007; Pineda et al. 2008; Royeck et al.  
531 2008). A common protocol used to measure total membrane capacitance is to integrate  
532 the transient capacitive current produced during voltage clamp steps (Haedo and  
533 Golowasch 2006; Iwasaki et al. 2008; Khorkova and Golowasch 2007; Pineda et al.  
534 2008; Royeck et al. 2008). This method is fast and simple to use and some  
535 electrophysiological data acquisition software includes an automatic capacitance  
536 calculation based on this method (e.g., pClamp, Molecular Devices). The application of  
537 this protocol is based on the crucial assumption that the cell is isopotential. Occasionally,  
538 this assumption is satisfied, such as with small cells with few or short processes. Another  
539 common method for measuring total membrane capacitance is to calculate the ratio of the  
540 membrane time constant, measured using current steps, to the cell input resistance. This  
541 method applies to an isopotential cell as well as a finite cable (or, using a correction  
542 factor, to a cable connected to a spherical soma) if the correct resistive term is used rather  
543 than the input resistance (Rall 1977). Other methods, such as applying a voltage ramp  
544 under voltage clamp conditions (Nadim et al. 1995) or phase-shift measurements in  
545 response to sine wave current inputs (Johnson et al. 2002; Joshi and Fernandez 1988;  
546 Neher and Marty 1982) can also be used to measure total membrane capacitance. A  
547 voltage ramp, for example, uses the fact that the capacitive current is proportional to the  
548 rate of change of the membrane potential with the constant of proportionality equal to the  
549 membrane capacitance (Eq. 4). All these methods are based on the theoretical assumption  
550 of isopotentiality or, alternatively, having a finite uniform cable structure. However, most  
551 biological neurons violate these assumptions and thus these methods can produce  
552 erroneous total membrane capacitance values.

553

554 In this paper we use identified neurons of the crab STG to demonstrate that three  
555 different protocols, the voltage clamp step, the current clamp step and voltage clamp  
556 ramps, yield significantly different capacitance values. We then use neuronal models of

557 varying architectures to examine which method produces a more accurate estimate of  
558 total membrane capacitance. The modeling results show that both voltage clamp methods  
559 produce significantly lower capacitance values than the current clamp method and that,  
560 for more complex neurons all methods underestimate the actual total membrane  
561 capacitance values. Using mathematical derivations of the transient solution to a current  
562 clamp pulse it can be shown that the slowest exponential term should provide an accurate  
563 estimate of total capacitance for any neuron independent of the anatomical complexity  
564 (Major et al. 1993a). Thus, it appears that the deviations from the actual capacitance  
565 observed using the current clamp method (Fig. 7A) stems from an increasingly large  
566 numerical error in the multi-exponential fits with increasingly complex architectures.  
567 However, the current clamp method produces extremely accurate estimates of a cell's  
568 total membrane capacitance even for highly complex architectures and a very large range  
569 of specific membrane resistivity values. For instance, high accuracy is obtained in a ball-  
570 cable-ball model (with the two balls representing the soma and the dendrite surfaces, e.g.  
571 Fig. 3A) for cable lengths up to  $1.25\lambda$  and a dendritic compartment of diameter  $200\mu\text{m}$ .  
572 The model shows that there is a trade-off in accuracy between the dendritic compartment  
573 size and cable length. With smaller dendritic compartments, accuracy is maintained even  
574 for longer cables (Fig. 4) whereas for shorter cables, accuracy is maintained for much  
575 larger dendritic compartments (Fig. 3B).

576

577 Similar accuracy levels can be obtained for neuron models with dendritic surface  
578 distributed over a tree of connected dendrites, even for neurons with several branching  
579 levels (Figs. 5, 6). The maximum total capacitance of our most complex model is similar  
580 to that of our ball-cable-ball model with a dendrite compartment diameter of  $200\mu\text{m}$  and  
581 a cable of only  $0.25\lambda$ . However, in contrast to the ball-cable-ball model, the capacitance  
582 estimates in this tree model are not as accurate even with the current clamp step method,  
583 indicating that the distributed capacitance over large electrotonic distances is partly  
584 responsible for the inaccuracy. At the same time, the capacitance load at the dendritic  
585 terminal also plays a role since different dendritic terminal sizes lumped into a simple  
586 sphere at the end of a fixed-length cable also yield different levels of accuracy.

587

588 Increasing the leakiness of the soma, such as produced by impalement damage, leads to  
589 an overestimate of the total membrane capacitance measurements with the current clamp  
590 step method. This suggests that an independent knowledge of the input resistance of an  
591 undamaged cell (such as can be obtained in the whole-cell patch clamp mode) can help  
592 set acceptable minimum input resistance levels to minimize capacitance estimate errors.  
593 In contrast, voltage clamp capacitance measurement methods are independent of soma  
594 damage, because with high enough gain the voltage clamp can inject sufficient current  
595 into the soma to overcome the increased membrane leak. The charging of the membrane  
596 capacitance can then proceed at the clamped voltage and thus the capacitive current  
597 remains unaffected. A different effect occurs when the overall membrane resistivity  $R_m$  is  
598 modified. The current clamp protocol estimate is only negatively affected at  $R_m$  values  
599 that are very low (below  $\sim 3,000 \Omega \cdot \text{cm}^2$ ), which are seldom encountered in neurons (but  
600 see (Hodgkin and Huxley 1952), while the voltage clamp protocol estimates deteriorate  
601 steeply with reduced  $R_m$ . Changing  $R_m$  also results in changing  $R_{in}$ , yet in contrast to the  
602 effect of soma leak conductance on  $R_{in}$ , there is little change in the measured total  
603 membrane capacitance with the current clamp method (Figs. 3C and 3D). The difference  
604 between these two effects is likely due to the fact that changing the soma leak  
605 conductance leads to different  $\tau_m$  values between the soma and the dendritic structure  
606 whereas changing  $R_m$  does not.

607

608 The distinct estimates of capacitance values provide information about the approximate  
609 distribution of surface area over the neuron's structure. In particular, while the current  
610 clamp estimate gives a total capacitance that is remarkably close to the actual capacitance  
611 of the cell (especially if the electrotonic length of the cell is relatively short, e.g.  $L < 2$ ),  
612 the voltage clamp protocols only yield estimates of the capacitance of the compartments  
613 near the site of current injection. The capacitance difference between these estimates  
614 corresponds to the capacitance of membrane located in distal compartments of the cell.  
615 However, the assumption that the current clamp step protocol always gives a correct  
616 estimate of the total neuronal capacitance is likely erroneous. Anatomical studies have  
617 shown that the LP and PD neurons have many long, fine dendrites (Bucher et al. 2007).  
618 The extremely large capacitance values we obtain in our current clamp protocols are

619 likely a reflection of the many thin and long dendrites these cells possess (cf. Figs. 4 and  
620 7 in (Bucher et al. 2007). Such dendrites may have large electrotonic lengths, and  
621 therefore current clamp measurements likely underestimate the total capacitance of these  
622 neurons, albeit by a lower degree than the voltage-clamp measurements, as our modeling  
623 experiments with complex neuron models that include multiple dendrites demonstrates.  
624 The role played by the presence of a long axon on these measurements depends on the  
625 location where the axon emerges, with more accurate estimates obtained in neurons  
626 resembling typical vertebrate CNS neurons, in which an axon often emerges directly  
627 from the soma.

628

629 The estimates from the three measurement protocols can be used to determine the  
630 approximate surface area distribution in a model that accounts for the neuron's spatial  
631 structure. As a result, even the simple ball-cable-ball model used in this study may  
632 provide a good approximation for the distribution of ion channel conductances over  
633 functionally distinct neuronal structures representing those of a biological neuron (e.g.  
634 soma and dendrites). We used the estimates of the total membrane capacitance of the PD  
635 and LP neurons obtained with the different measurement protocols to predict the relative  
636 distribution of surface areas over functionally relevant compartments of these cells (Fig.  
637 3B). Our results suggest that the compartment distal from the recording site has a surface  
638 area at least 15 to 25 times larger than the near compartment. We emphasize that this  
639 result does not imply that the near compartment corresponds to the soma and the distal  
640 compartment to the rest of the neuron's membrane. Indeed, exact inferences of total  
641 dendritic surface distribution cannot be made from such a simple comparison but would  
642 require a combination of accurate anatomical and physiological measurements. Yet, the  
643 ratio of the CC-measured capacitance to the VC-measured capacitance in different cells  
644 can provide an estimate of the relative sizes of the dendritic surface area in different  
645 neurons (Fig. 3B). From such measurements we can conclude that PD neurons appear to  
646 have a larger "dendritic" surface area than LP neurons. This may be a reflection of an  
647 extended surface area due to strong gap junctions between the PD neuron and other  
648 neurons to which it is strongly coupled (see (Rabbah et al. 2005); this additional surface

649 area that would be absent in the LP neuron which has much weaker gap junctional  
650 connections.

651

652 Another difficulty with capacitance estimation is deciding the part of the cell surface to  
653 use for estimating the capacitance. If studying changes in membrane surface area as a  
654 result of growth or degeneration, total capacitance would likely be the appropriate choice.  
655 If seeking to normalize measurements of voltage-gated conductances, the choice is less  
656 clear. In this case, one would like to measure a capacitance that reflects the portion of  
657 membrane that contributes to the measured voltage-clamp current. However, it is not  
658 clear that such a specialized portion of the membrane is a well-defined notion, because a  
659 voltage-clamp step applied to the soma affects the voltage of a patch of membrane to a  
660 greater or lesser extent depending on the electrotonic distance from the soma to that  
661 patch. Here we have focused on measuring the *total* capacitance of the membrane, and  
662 our results imply that voltage-clamp measurements provide a poor estimate of the total  
663 capacitance.

664

665 Because the membrane time constant is a property of the membrane and not of  
666 geometrical factors, it is equal to the product of the actual capacitance and resistance of  
667 the membrane or of the specific membrane capacitance and resistivity,  $\tau_m = r_m c_m = R_m C_m$ .  
668 The specific membrane capacitance of most neurons falls in the range of 0.5-1.0  $\mu\text{F}/\text{cm}^2$   
669 (Koch 1999; Solsona et al. 1998). Table 1 shows that the time constants of PD and LP  
670 neurons are approximately 155 and 220 msec, respectively. Thus, even with the more  
671 conservative value of  $C_m=1.0 \mu\text{F}/\text{cm}^2$ , the specific membrane resistivity of these cells is  
672 at least 155 and 220  $\text{k}\Omega\text{cm}^2$ , respectively, which is over three-fold higher than previously  
673 thought (Nadim and Golowasch 2006; Rabbah et al. 2005). It remains to be determined  
674 how this difference may impact the behavior of existing models of LP and PD neurons  
675 (Golowasch and Marder 1992; Soto-Trevino et al. 2005).

676

677 Although our study is restricted to the three methods described above, alternative  
678 methods for measuring total membrane capacitance exist based on the frequency-  
679 dependent impedance measured in response to sinusoidal current inputs. This dependency

680 is applied, for example, by lock-in amplifiers for capacitance measurements, and has  
681 been used to measure membrane surface changes during exocytosis (Johnson et al. 2002;  
682 Joshi and Fernandez 1988; Neher and Marty 1982). This method also assumes a compact  
683 cell structure and suffers from similar limitations as those found with the current clamp  
684 step method. The current clamp step method allows for a straightforward decomposition  
685 of the voltage response in the form of multiple exponential terms, with one of these terms  
686 (the slowest) corresponding to the charging of the membrane capacitance. The two  
687 parameters (amplitude and time constant) of this slow exponential term can then be used  
688 to calculate the total membrane capacitance. A different current clamp protocol that uses  
689 a continuously varying frequency sinusoidal current injection (ZAP function) also allows  
690 the determination of the slow membrane time constant and thus membrane capacitance  
691 using a similar decomposition into multiple terms (Puil et al. 1986).

692 Capacitance measurements are often used to determine the conductance density of ionic  
693 currents. Although the electrotonic structure of the neuron affects the accuracy of the  
694 measured total membrane capacitance, these effects are probably not the same as space  
695 clamp errors produced when measuring voltage-gated ionic conductances. Capacitance  
696 measurements are ideally conducted in the linear range of membrane potential near the  
697 resting potential and thus membrane conductance changes do not play any role. In  
698 contrast, when voltage-gated channels are activated, the membrane potential is affected  
699 both by the electrotonic structure, which can be significantly different from the resting  
700 electrotonic structure due to conductance activation, and by additional loss of voltage  
701 control due to the nonlinear conductance changes. In fact, the loss of voltage control due  
702 to space clamp errors leads to the underestimation of outward currents, but leads to  
703 under- or over-estimates of inward currents that depend on the membrane potential, the  
704 overestimates being due to the regenerative effects of inward currents on the membrane  
705 potential at distant regions (e.g. (Hartline and Castelfranco 2003). As a consequence of  
706 the well-known anisotropy of ion channel distribution, most salient for synaptic contacts,  
707 normalizing conductance measurements to total membrane capacitance measurements  
708 needs to be performed with caution, even if the total cell surface area is accurately  
709 determined. Accurate measurement of dendritic capacitance, voltage-gated currents, and  
710 synaptic currents are all likely to be compromised by space clamp problems.

711

712 The accuracy of capacitance measurements is sensitive to the quality of the recordings.  
713 Noise has a modest effect in our models (e.g., 5% white noise introduces <1% error in  
714 our current clamp step protocol estimates). However, signal transients, drifts and other  
715 unstable behavior can significantly affect the estimates obtained with all of these  
716 protocols particularly if voltage-gated currents are activated. Slow changes in the  
717 membrane potential will greatly affect capacitance measurements using the current clamp  
718 protocol since it relies on an accurate estimation of the slowest time constant. In contrast,  
719 fast signal changes primarily affect voltage clamp step protocol estimates of capacitance.  
720 Low sampling rates (aliasing) can greatly reduce the accuracy of the measurements in  
721 voltage clamp, especially with the voltage clamp step protocol. The accuracy and the rate  
722 of the membrane potential change during a voltage clamp step increases with an increase  
723 in the voltage clamp gain. However, as the rate of voltage change increases, a fixed low  
724 sampling rate may introduce aliasing effects that will result in the underestimation of the  
725 total measured charge and thus the capacitance estimate. The voltage clamp step protocol  
726 therefore requires high sampling rates depending on the voltage clamp gain. In contrast,  
727 current clamp measurements would not be as affected by aliasing problems. Short  
728 duration voltage clamp steps are usually used when this method is preferred under the  
729 assumption that the membrane capacitance charges quickly. This is indeed the case in  
730 isopotential cells, especially if the clamp gain is set high. However, in non-isopotential  
731 cells, there is significant current flow into distal compartments, and charging of the  
732 capacitor of such distal compartments takes time and is influenced by the axial resistance  
733 between the proximal and distal compartments (Eq. 11, see Appendix). Therefore, longer  
734 voltage clamp pulses will yield larger (and more accurate) estimates of the total  
735 membrane capacitance.

736

737 The discrepancy between estimated capacitance values in current- versus voltage-clamp  
738 methods can intuitively be understood as follows: voltage clamp methods control the  
739 membrane potential of a restricted area of the membrane near the electrode.  
740 Electrotonically distant regions, however, are not clamped to the same voltage due to lack  
741 of space clamp (Breneman et al. 2008; Prinz and Fromherz 2003; Spruston et al. 1993).

742 The errors in the total membrane capacitance estimates originate from the assumption  
743 that the clamped membrane potential measured at the point of electrode penetration is  
744 maintained throughout the cell surface. Since the voltage difference drops with distance,  
745 less charge accumulates at distant points than would accumulate if the voltage at these  
746 distant points was the same as that imposed at the soma, hence the underestimate. The  
747 lack of space clamp also explains why voltage clamp ramp capacitance estimates depend  
748 on the slope of the membrane potential change. At higher  $dV/dt$  values, the membrane  
749 potential in distant regions differs more from that of the point of penetration due to the  
750 membrane filtering properties thus producing larger errors in the capacitance estimates.  
751 The same argument explains why the fast voltage clamp ramps lead to larger errors than  
752 voltage clamp steps. In the Appendix we provide a derivation of equations for the simple  
753 two-compartment model shown in Fig. 8A that shows that the contribution of distal  
754 compartments is identically affected in both voltage clamp methods by the electrotonic  
755 distance of the soma to this compartment (represented by the resistance  $R_a$ ) and the  
756 leakiness of the distal compartment (represented by  $R_f$ ; Eqs. A25 and A31). The methods  
757 depend differently on the duration of the voltage clamp steps and ramps. However, these  
758 equations clearly show that long voltage pulses and slow voltage ramps are necessary to  
759 minimize the capacitance measurement errors when using these methods.

760

761 The charge from a current step is rapidly equalized throughout the cell structure, but  
762 affects the average membrane potential more slowly. This can be seen, for example, in  
763 the equations describing membrane potential in a finite cable with a sealed end (Eq. 1),  
764 which is given by an infinite series of exponentially decaying terms, the slowest of which  
765 corresponds to the membrane time constant (Holmes et al. 1992; Rall 1977). Although  
766 for very long cables this description breaks down, it still holds for finite cables of varying  
767 terminating resistances (Holmes et al. 1992; Rall 1977), which explains the accuracy of  
768 the capacitance measurements in cells that can be described with a ball-cable-ball  
769 as long as the cable is not excessively long (see Fig. 4).

770

771 In summary, our results show that membrane capacitance can be measured with  
772 remarkable accuracy using the current clamp step method even in cells with complex

773 architectures. With highly complex neurons the current clamp step method can  
774 underestimate the capacitance due to numerical errors introduced by multi-exponential  
775 fitting methods. It is important to note again that the voltage amplitude term  $V_0$  in Eq. 1  
776 divided by the input current corresponds to a resistive term that must be used to calculate  
777 the total membrane capacitance. The input resistance of the cell, which is often used  
778 instead, is the incorrect parameter to use in non-isopotential cells. On the other hand, the  
779 methods most commonly used to measure capacitance (voltage clamp step or ramp  
780 protocols) yield significant errors for neurons whose membrane structure is not  
781 electrotonically compact and should be used with caution. When measurements are done  
782 with current as well as voltage clamp steps, long pulses should be used, rather than brief  
783 pulses, as is commonly done in particular with voltage clamp pulses.

784

785

#### 786 **Acknowledgments**

787 This work was supported by NSF UBM Training Grant DUE-0436244, and NIH grants  
788 MH64711 (JG), MH60605 (FN), NS50928 (ALT), and MH46742 (ALT).

789 **Appendix. A two-compartment model**

790

791 We would like to demonstrate that the current clamp estimate of the total membrane  
 792 capacitance is a good approximation (and that the voltage clamp estimates deviate from  
 793 this value) to the actual total capacitance of our simplest model in which two spheres, one  
 794 representing the soma (the “near” compartment, characterized by  $C_n$  and  $R_n$ ) and one  
 795 representing the dendrite (the “far” compartment, characterized by  $C_f$  and  $R_f$ ) are coupled  
 796 by a simple resistor  $R_a$ , representing the resistance of a cable-like structure such as a  
 797 neurite (Fig. 8). The current clamp estimate of capacitance is given by  $\tau_0 / R_0$ , where  $\tau_0$   
 798 and  $R_0$  are as defined in Eq. 1 above. It has been shown before that capacitance can be  
 799 determined accurately in this manner for neurons of arbitrarily complex architectures, at  
 800 least in the absence of somatic shunt (Major et al. 1993a). Our goal is to derive values for  
 801 these quantities in terms of the circuit parameters that can provide a clear and intuitive  
 802 understanding of the sources of error when using the voltage clamp protocols described  
 803 in this paper. We begin with  $\tau_0$ . The input impedance of the cell can be written as  
 804 (Siebert 1986)

805

806 
$$Z(s) = \frac{1}{\frac{1}{R_n} + C_n s + \frac{1}{R_a + \frac{1}{\frac{1}{R_f} + C_f s}}} \quad (\text{A1})$$

807

808 where  $s$  is the complex frequency. The right side of this equation can be rearranged,  
 809 yielding

810

811 
$$Z(s) = \frac{\frac{R_a R_n + R_f R_n}{R_a + R_f + R_n} + \frac{C_f R_a R_f R_n}{R_a + R_f + R_n} s}{1 + \frac{C_f R_a R_f + C_n R_a R_n + C_f R_f R_n + C_n R_f R_n}{R_a + R_f + R_n} s + \frac{C_n C_f R_a R_n R_f}{R_a + R_f + R_n} s^2} \quad (\text{A2})$$

812

813

814 The impedance of a system that responds to a current step in the manner described by  
 815 Eq. 8 is given by the expression (Siebert 1986)

816

$$817 \quad Z(s) = \frac{R_0}{1 + \tau_0 s} + \frac{R_1}{1 + \tau_1 s} \quad (\text{A3})$$

818

819 multiplying this out and rearranging, we obtain

820

$$821 \quad Z(s) = \frac{(R_0 + R_1) + (R_1 \tau_0 + R_1 \tau_1)s}{1 + (\tau_0 + \tau_1)s + \tau_0 \tau_1 s^2} \quad (\text{A4})$$

822

823 Eq. A4 has the same form as Eq. A2, and so we can infer that the coefficients of each  
 824 term for  $Z(s)$  must be identical. Thus we write a system of four equations relating the  
 825 circuit parameters ( $C_n$ ,  $C_f$ ,  $R_n$ ,  $R_f$ ,  $R_a$ ) to the “kernel” parameters ( $R_0$ ,  $\tau_0$ ,  $R_1$ ,  $\tau_1$ ):

826

827 If we assume that  $R_n C_n = R_f C_f$ , as would be the case for a cell with uniform specific  
 828 membrane conductance and capacitance, this adds a fifth equation to this system and we  
 829 can define a common time constant  $\tau_c = R_n C_n = R_f C_f$ , yielding

830

$$831 \quad R_0 + R_1 = \frac{R_a R_n + R_f R_n}{R_a + R_f + R_n} \quad (\text{A5})$$

$$832 \quad R_0 \tau_1 + R_1 \tau_0 = \frac{R_a R_n \tau_c}{R_a + R_f + R_n} \quad (\text{A6})$$

$$833 \quad \tau_0 + \tau_1 = \frac{(R_n + 2R_a + R_f) \tau_c}{R_a + R_f + R_n} \quad (\text{A7})$$

$$834 \quad \tau_0 \tau_1 = \frac{R_a \tau_c^2}{R_a + R_f + R_n} \quad (\text{A8})$$

835

836 Equations A7 and A8 comprise a system of two equations in the two unknowns  $\tau_0$  and  $\tau_1$   
 837 that can be reduced to a single quadratic equation in  $\tau_0$ . Since Eqs. A7 and A8 are

838 symmetric in  $\tau_0$  and  $\tau_1$ , we adopt the standard convention that  $\tau_0$  is the larger of the two.

839 Thus

840

$$841 \quad \tau_0 = \frac{\Gamma + \sqrt{\Gamma^2 - 4\Delta}}{2} \quad (\text{A9})$$

$$842 \quad \tau_1 = \frac{\Gamma - \sqrt{\Gamma^2 - 4\Delta}}{2} \quad (\text{A10})$$

843

$$844 \quad \text{where } \Gamma = \frac{(R_n + 2R_a + R_f)\tau_c}{R_a + R_f + R_n}, \text{ and } \Delta = \frac{R_a\tau_c^2}{R_a + R_f + R_n}.$$

845

846 After some algebra, this reduces to

847

$$848 \quad \tau_0 = \tau_c \quad (\text{A11})$$

$$849 \quad \tau_1 = \frac{R_a}{R_a + R_f + R_n} \tau_c \quad (\text{A12})$$

850

851 Next we solve Eqs. A5 and A6 using Eqs. A11 and A12 for  $R_0$  and  $R_1$ , yielding

852

$$853 \quad R_0 = \frac{1}{R_n^{-1} + R_f^{-1}} \quad (\text{A13})$$

$$854 \quad R_1 = \frac{R_a R_n^2}{(R_n + R_f)(R_a + R_f + R_n)} \quad (\text{A14})$$

855

856 As for  $\tau_0$  and  $\tau_1$ ,  $R_0$  and  $R_1$  are expressed in terms of circuit parameters. Using Eqs. A11

857 and A13, the current-clamp estimate of capacitance is thus given by

858

$$859 \quad c_{m,ic} = \frac{\tau_0}{R_0} = \tau_c (R_n^{-1} + R_f^{-1}) = C_n + C_f \quad (\text{A15})$$

860

861 This shows that, for the simple case of a two-compartment model in which the near and  
 862 the distant compartments are coupled by a resistor only (rather than a cable) the current  
 863 clamp method gives an accurate measurement of the total capacitance.

864

865 Next we derive the response of the two-compartment model to a voltage-clamp step  
 866  $v(t) = \Delta V_m$  (see Eq. 10). Using Eq. A4, the current response of the system is given by

867

$$\begin{aligned}
 I(s) &= \frac{V(s)}{Z(s)} \\
 868 \quad &= \Delta V_m \frac{1 + (\tau_0 + \tau_1)s + \tau_0\tau_1s^2}{(R_0 + R_1)s + (R_1\tau_0 + R_0\tau_1)s^2} \tag{A16} \\
 &= \Delta V_m \left[ \frac{\tau_0\tau_1}{R_1\tau_0 + R_0\tau_1} + \frac{(R_0 + R_1)^{-1}}{s} + \frac{\frac{R_0R_1(\tau_0 - \tau_1)^2}{(R_0 + R_1)(R_1\tau_0 + R_0\tau_1)^2}}{s + \frac{R_0 + R_1}{R_1\tau_0 + R_0\tau_1}} \right]
 \end{aligned}$$

869

870 The current response is given by the inverse Laplace transform of  $I(s)$ , and can be  
 871 written as

872

$$873 \quad I(t) = \Delta V_m \left[ c_{pulse} \delta(t) + G_m u(t) + G_{decay} u(t) \exp\left(-\frac{t}{\tau_{vc}}\right) \right] \tag{A17}$$

874

875 where

876

$$877 \quad c_{pulse} = \frac{\tau_0\tau_1}{R_1\tau_0 + R_0\tau_1} \tag{A18}$$

$$878 \quad G_m = (R_0 + R_1)^{-1} \tag{A19}$$

$$879 \quad G_{decay} = \frac{R_0R_1(\tau_0 - \tau_1)^2}{(R_0 + R_1)(R_1\tau_0 + R_0\tau_1)^2} \tag{A20}$$

$$880 \quad \tau_{vc} = \frac{R_1\tau_0 + R_0\tau_1}{R_0 + R_1} \tag{A21}$$

881

882 The charge delivered by the transient part of Eq. A17 is given by

883

$$\begin{aligned}
 884 \quad Q &= \int_0^{t_p} \Delta V_m \left[ c_{pulse} \delta(t) + u(t) G_{decay} \exp\left(-\frac{t}{\tau_{vc}}\right) \right] dt \\
 &= \Delta V_m \left[ c_{pulse} + G_{decay} \tau_{vc} \left( 1 - \exp\left(-\frac{t_p}{\tau_{vc}}\right) \right) \right]
 \end{aligned} \tag{A22}$$

885

886 Dividing out by  $\Delta V_m$  yields the estimate of capacitance using a voltage-clamp step

887

$$888 \quad c_{m,vc} = c_{pulse} + G_{decay} \tau_{vc} \left( 1 - \exp\left(-\frac{t_p}{\tau_{vc}}\right) \right) \tag{A23}$$

889

890 This equation clearly shows that the estimate of  $c_{m,vc}$  depends on the duration of the  
 891 voltage pulse,  $t_p$ , with very short pulses yielding an estimate of  $c_{m,vc} = c_{pulse}$ , which after  
 892 substitution in terms of circuit parameters simplifies to  $c_{m,vc} = C_n$ , i.e. the capacitance of  
 893 the near compartment only. For very long pulses, the exponential term approaches zero  
 894 and  $c_{m,vc} = c_{pulse} + G_{decay} \tau_{vc}$ , which can be written in terms of the kernel parameters ( $R_0$ ,  $\tau_0$ ,  $R_l$ ,  
 895  $\tau_l$ ) by substitution, using Eqs. A18, A20, and A21:

896

$$897 \quad c_{m,vc} = \frac{R_0 \tau_0 + R_l \tau_l}{(R_0 + R_l)^2} \tag{A24}$$

898

899 Substituting in the expressions for  $\tau_0$ ,  $\tau_l$ ,  $R_0$ , and  $R_l$  in terms of circuit parameters  
 900 (Eqs. A11-A14) and simplifying leads to

901

$$\begin{aligned}
 902 \quad c_{m,vc} &= \frac{\tau_c}{R_n} + \frac{\tau_c}{R_f} \cdot \frac{1}{(1 + R_a / R_f)^2} \\
 &= C_n + C_f \frac{1}{(1 + R_a / R_f)^2}
 \end{aligned} \tag{A25}$$

903

904 which is Eq. 11. Equations A23 and A25 show that the total capacitance measured using  
 905 the voltage-clamp step protocol strongly depends on the duration of the voltage pulse, but

906 is also dominated by the capacitance of the near compartment (typically the soma),  
 907 especially for large values of axial (coupling) resistance  $R_a$ . The contribution from the far  
 908 compartment drops as either the resistance of the far compartment,  $R_f$ , decreases, [e.g. if  
 909 its surface increases (Fig. 3)] or  $R_a$  increases (e.g. if the neurite gets longer) (Fig. 4C).

910  
 911 Another way of looking at the error generated when using the voltage clamp protocol is  
 912 to calculate the ratio of the VC\_step estimate to the CC\_step estimate in terms of the  
 913 kernel parameters ( $R_0$ ,  $\tau_0$ ,  $R_1$ ,  $\tau_1$ ). The ratio can be defined (using Eqs. A15 and A24) as  
 914

$$915 \quad \frac{c_{m,vc}}{c_{m,ic}} = \frac{R_0^2 + \frac{R_0 R_1 \tau_1}{\tau_0}}{R_m^2} \quad \text{where } R_m = R_0 + R_1. \quad (A26)$$

916  
 917 A similar approach can be used to derive the response of our two-compartment model  
 918 (Fig. 8A) to a voltage clamp ramp. To determine the total membrane capacitance we first  
 919 find the response of the circuit to a single voltage ramp given by  $v_{ramp}(t) = m \cdot t \cdot u(t)$ , where  
 920  $m$  is the slope of the ramp and  $u(t)$  is a step function as before. The response of the circuit  
 921 can be shown, via Laplace transforms, to be

$$922 \quad i_{ramp}(t) = \left[ \frac{-R_0(t + \tau_0) - R_1(t + \tau_1) + \frac{R_0 R_1 (\tau_0 - \tau_1)^2}{R_1 \tau_0 + R_0 \tau_1} \exp\left(-\frac{t}{\frac{R_1 \tau_0 + R_0 \tau_1}{R_0 + R_1}}\right)}{(R_0 + R_1)^2} \right] \cdot m \cdot u(t) \quad (A27)$$

924  
 925 In our VC\_ramp protocol, a depolarizing voltage ramp is followed by an identical  
 926 hyperpolarizing ramp. The capacitance estimate in this case is given by

927

928 
$$C_{ramp} = \frac{i_{hyp} - i_{dep}}{2m}$$

929 
$$= \frac{i\left(\frac{T}{2}\right) - i\left(\frac{3T}{2}\right)}{2m}$$
 (A28)

929 if we sample the current at the midpoint of both ramps ( $T$  is the ramp duration). Since the  
 930 system is linear and shift-invariant, the current response of the system can be written:  
 931

932 
$$i(t) = i_{ramp}(t) - 2 \cdot i_{ramp}(t-T) + i_{ramp}(t-2T)$$
 (A29)

933

934 Combining Eqs. A27, A28 and A29 and simplifying yields

935

$$c_{ramp}(T) = \frac{\frac{1}{2}\sqrt{\beta}(\beta-3) + \frac{(R_0\tau_0 + R_1\tau_1)(R_1\tau_0 + R_0\tau_1)}{R_0R_1(\tau_0 - \tau_1)^2}}{(R_0 + R_1)^2}$$

936 where (A30)

$$\beta = \exp\left(-\frac{(R_0 + R_1)T}{R_1\tau_0 + R_0\tau_1}\right)$$

937

938 Substituting kernel with circuit parameters (and  $T$  with  $\Delta V_{ramp}/m$ , where  $\Delta V_{ramp}$  is the  
 939 amplitude of the ramp), this expression becomes

940

$$c_{ramp}(m) = C_n + C_f \left(\frac{1}{1 + R_a / R_f}\right)^2 \left[\frac{1}{2}\sqrt{\beta}(\beta-3) + 1\right]$$

941 and (A31)

$$\beta = \exp\left(-\frac{\Delta V_{ramp}}{m \cdot C_f} \left(\frac{1}{R_a} + \frac{1}{R_f}\right)\right)$$

942

943 Notice that when  $m$  is large, i.e. a ramp is very fast, the term  $\frac{1}{2}\sqrt{\beta}(\beta-3) + 1$  tends to zero,

944 and the capacitance estimate reduces to that of the near compartment only, just as with

945 very short voltage clamp steps. With very small  $m$ , the term  $\frac{1}{2}\sqrt{\beta}(\beta-3) + 1$  tends to 1,

946 and we obtain the same expression as with long voltage clamp steps, as shown  
947 numerically in Fig. 3B for the ball-stick-ball model (compare green, red lines).  
948

949

950 **Figure Legends**

951

952 **Figure 1.** *Total membrane capacitance measurement protocols.* Schematic diagrams  
953 representing the protocols used. **A.** *Current clamp step.* The membrane potential change  
954 (black trace) elicited by a 1 sec long current step ( $I_{ext}$ ) was fitted with two exponentials  
955 (grey traces). The slowest component corresponds to the charging of the membrane  
956 capacitor. **B.** *Voltage clamp step.* The area under the capacitive current transient (grey) is  
957 the charge deposited on the membrane for a given  $\Delta V_m$ . The duration of this pulse is  
958 typically shorter than the current clamp steps. **C.** *Voltage clamp ramp.* Membrane  
959 potential ramps elicit a capacitive current step  $I_C$ . The sign of  $I_C$  depends on the slope of  
960 the voltage ramp. If a symmetric voltage ramp is used, the difference between the values  
961 of  $I_m$  measured at the same membrane potential during the up and down ramps is equal to  
962  $2I_C$ . This value was calculated by measuring the average current value of the upper and  
963 the lower branches over the grayed area in the I-V-curve and dividing by  $2 \times dV/dt$  (see  
964 Methods; arrows correspond to the slope of the voltage ramp).

965

966 **Figure 2.** *Effect of experimental protocol on total membrane capacitance measurements.*  
967 PD and LP neurons were impaled with two electrodes and capacitance measured in either  
968 current clamp (CC\_step) or voltage clamp (VC\_step or VC\_ramp) in the presence of  
969 TTX and  $Cs^+$  in the bath as described in Methods. The capacitance values were compared  
970 with a Kruskal-Wallis One-way ANOVA on Ranks with post-hoc Dunn's test  
971 comparisons. \*\*\*  $P < 0.001$ . More details in Table I.

972

973 **Figure 3.** *Effect of measurement protocol on total membrane capacitance estimates in a*  
974 *simple neuronal model.* **A.** Diagram of the model cell. The length of the neurite is  $0.25\lambda$ .  
975 **B.** The capacitance in the model was determined with the three protocols described in  
976 Methods, and with two ramp slopes. Values were normalized against the actual total  
977 capacitance of the cell and are plotted against the diameter of the dendritic compartment.  
978 Normalized capacitance values measured in PD neurons ( $n = 29$ ) and LP neurons ( $n = 19$ )  
979 using the same protocols as in the model. Capacitance values of each PD and LP neuron

980 recorded were normalized to the neuron's own current clamp-measured capacitance  
981 (Table I). **C.** Dependence of the measurements on soma and input resistance. The model  
982 cell shown in A with a dendrite diameter of 400  $\mu\text{m}$  was used, and the conductance of the  
983 soma compartment was varied (0.5 to 125 nS). The capacitance was measured with the  
984 CC\_step and VC\_step methods in response to 1-sec long current and voltage pulses  
985 respectively, and normalized by the actual cell capacitance. The input resistance  $R_{in}$  was  
986 measured using Ohm's law. **D.** Dependence of the measurements on specific membrane  
987 resistivity. The model cell shown in A with a dendrite diameter of 400  $\mu\text{m}$  was used, and  
988 current clamp and voltage clamp pulses of 1-sec duration were used. As in B, measured  
989 capacitance values were normalized against the actual total capacitance of the cell and are  
990 plotted against the specific membrane resistivity  $R_m$ .

991

992 **Figure 4.** *Effect of distance of the dendritic compartment from the point of recording.* A  
993 model identical to that used in Fig. 3 was used but the dendritic diameter was fixed at 4  
994 different values and the length of the neurite varied, and plotted as the electrotonic length.  
995 Measured capacitance was normalized by the actual total cell capacitance.

996

997 **Figure 5.** *Effect of cell architecture on total membrane capacitance estimates.*

998 Capacitance was measured using either the current clamp (CC\_step; filled symbols) or  
999 voltage clamp step protocols (VC\_step; open symbols) and is graphed without  
1000 normalization. The actual capacitance was determined from the surface of the cell and the  
1001 specific membrane capacitance. **A.** Asymmetric tree. The inset illustrates the architecture  
1002 of this model: each subsequent dendritic level has a maximum of double the number of  
1003 dendrites of the preceding level, and all branches at any given level emerge from a single  
1004 dendrite. **B.** Concentric tree. The same dendrites as in A, all emerge directly from the  
1005 soma. **C.** Comparison of the data from the asymmetric tree (from A) and data from a  
1006 "symmetric tree" in which the same branches as in A emerge symmetrically from the  
1007 previous level (see text).

1008

1009 **Figure 6.** *Effect of the presence of an axon on total membrane capacitance estimates.*

1010 Capacitance was measured using the current clamp (CC\_step; filled symbols) and voltage

1011 clamp step protocols (VC\_step; open symbols) as described in Methods using 1-sec long  
1012 pulses in both cases. The model used was identical to that described in Fig. 5C except  
1013 that axons of different lengths and 10  $\mu\text{m}$  diameter were added at the end of one of the  
1014 two secondary dendrites (A) or to the soma (B).

1015

1016 **Figure 7.** *Effect of cell complexity on capacitance estimates.* A measurement error was  
1017 calculated as  $(C_m \text{ actual} - C_m \text{ measured}) / C_m \text{ actual}$  and plotted against a complexity  
1018 index that corresponds to the sum of the dendritic electrotonic lengths of all the branches  
1019 in the model. The asymmetric (A) and concentric (B) models described in Fig. 5 are  
1020 compared.

1021

1022 **Figure 8.** *Analytical estimates of capacitance in a two-compartment equivalent circuit of*  
1023 *the ball-stick-ball neuron model.* **A.** Diagram and equivalent circuit representation of a  
1024 two-compartment ball-stick-ball neuron.  $V_n$  denotes the membrane potential in the soma  
1025 (near) compartment and  $V_f$  the membrane potential in the distal (far) compartment (both  
1026 are offset by the resting potential, e.g.  $V_n = V_{mn} - V_{rest}$ ), coupled to the soma with  
1027 resistance  $R_d$ . The electrode in the soma represents the site of current injection ( $I_{ext}$ ) in  
1028 current or voltage clamp recording mode. **B.** Capacitance measurements normalized by  
1029 the actual total capacitance of the cell are plotted against the diameter of the distal  
1030 compartment  $d_d$  of the ball-stick-ball model neuron used before (inset). Measurements  
1031 labeled “VC\_step model” were obtained with the voltage clamp step protocol applied to  
1032 the ball-stick-ball model and are identical to those shown in Fig. 3B. Measurements  
1033 labeled “VC\_step analytical” were calculated using Eq. A26 and parameters  $R_0$ ,  $R_1$ ,  $\tau_0$   
1034 and  $\tau_1$  determined from 2-exponential fits to CC\_step data using the same ball-stick-ball  
1035 model.

1036 **Tables**

1037

1038 *Table 1. Capacitance values of PD and LP neurons obtained with different protocols.*

1039

Protocol	PD neuron capacitance (nF)			LP neuron capacitance (nF)		
	Average	SDev	N	Average	SDev	N
CC_step	65.61	68.23	29	83.82	50.71	18
VC_step	2.53	0.68	30	5.23	4.23	18
VC_ramp ( $dV/dt =$ 0.02mV/msec)	3.57	1.37	29	5.48	3.41	18
VC_ramp ( $dV/dt = 0.5$ mV/msec)	1.24	0.18	32	2.03	1.18	18

1040

1041 The average values of  $\tau_m$ ,  $\tau_I$ ,  $R_0$  and  $R_{in}$  for the PD neuron were  $158.7 \pm 96.4$  msec,  $33.9 \pm$   
 1042  $17.0$  msec,  $2.3 \pm 1.7$  M $\Omega$  and  $11.4 \pm 6.0$  M $\Omega$ , respectively (N = 29). The average values  
 1043 of  $\tau_m$ ,  $\tau_I$ ,  $R_0$  and  $R_{in}$  for the LP neuron were  $215.2 \pm 67.1$  msec,  $29.0 \pm 10.3$  msec,  $2.1 \pm$   
 1044  $0.9$  M $\Omega$  and  $9.7 \pm 6.8$  M $\Omega$ , respectively (N = 18). A post-hoc analysis with Dunn's  
 1045 Method showed that the CC\_step estimate is significantly higher ( $P < 0.001$ ) than either  
 1046 of the two voltage clamp methods, and that the capacitance estimate with the fast voltage  
 1047 clamp ramp method (0.5 mV/msec) is significantly ( $P < 0.001$ ) different from that with  
 1048 either VC\_step or slow (0.02 mV/msec) voltage clamp ramp method. The capacitance  
 1049 estimates with VC\_step and slow (0.02 mV/msec) voltage clamp ramp protocols are not  
 1050 significantly different.

1051

1052

1053 **References**

1054

- 1055 Breneman KD, Highstein SM, Boyle RD, and Rabbitt RD. The Passive Cable Properties  
1056 of Hair Cell Stereocilia and Their Contribution to Somatic Capacitance Measurements.  
1057 *Biophys J* 2008.
- 1058 Bucher D, Johnson CD, and Marder E. Neuronal morphology and neuropil structure in  
1059 the stomatogastric ganglion of the lobster, *Homarus americanus*. *J Comp Neurol* 501:  
1060 185-205, 2007.
- 1061 Chklovskii DB, Mel BW, and Svoboda K. Cortical rewiring and information storage.  
1062 *Nature* 431: 782-788, 2004.
- 1063 Dougherty KJ, Sawchuk MA, and Hochman S. Properties of mouse spinal lamina I  
1064 GABAergic interneurons. *J Neurophysiol* 94: 3221-3227, 2005.
- 1065 Golowasch J, and Marder E. Ionic currents of the lateral pyloric neuron of the  
1066 stomatogastric ganglion of the crab. *J Neurophysiol* 67: 318-331., 1992.
- 1067 Haedo RJ, and Golowasch J. Ionic mechanism underlying recovery of rhythmic activity  
1068 in adult isolated neurons. *J Neurophysiol* 96: 1860-1876, 2006.
- 1069 Harris-Warrick RM. *Dynamic biological networks : the stomatogastric nervous system*.  
1070 Cambridge, Mass.: MIT Press, 1992, p. xvii, 328.
- 1071 Harris FJ. *Multirate Signal Processing for Communication Systems*. Upper Saddle River,  
1072 NJ: Prentice Hall PTR, 2006.
- 1073 Hartline DK, and Castelfranco AM. Simulations of voltage clamping poorly space-  
1074 clamped voltage-dependent conductances in a uniform cylindrical neurite. *J Comput*  
1075 *Neurosci* 14: 253-269, 2003.
- 1076 Hodgkin AL, and Huxley AF. A quantitative description of membrane current and its  
1077 application to conduction and excitation in nerve. *J Physiol* 117: 500-544, 1952.
- 1078 Holmes WR, Segev I, and Rall W. Interpretation of time constant and electrotonic length  
1079 estimates in multicylinder or branched neuronal structures. *J Neurophysiol* 68: 1401-  
1080 1420, 1992.
- 1081 Iwasaki S, Chihara Y, Komuta Y, Ito K, and Sahara Y. Low-voltage-activated potassium  
1082 channels underlie the regulation of intrinsic firing properties of rat vestibular ganglion  
1083 cells. *J Neurophysiol* 100: 2192-2204, 2008.
- 1084 Johnson SL, Thomas MV, and Kros CJ. Membrane capacitance measurement using patch  
1085 clamp with integrated self-balancing lock-in amplifier. *Pflugers Arch* 443: 653-663,  
1086 2002.
- 1087 Joshi C, and Fernandez JM. Capacitance measurements. An analysis of the phase detector  
1088 technique used to study exocytosis and endocytosis. *Biophys J* 53: 885-892, 1988.
- 1089 Khorkova O, and Golowasch J. Neuromodulators, not activity, control coordinated  
1090 expression of ionic currents. *J Neurosci* 27: 8709-8718, 2007.
- 1091 Koch C. *Biophysics of Computation: Information Processing in Single Neurons*. Oxford  
1092 University Press, Inc., 1999.
- 1093 Major G, Evans JD, and Jack JJ. Solutions for transients in arbitrarily branching cables: I.  
1094 Voltage recording with a somatic shunt. *Biophys J* 65: 423-449, 1993a.
- 1095 Major G, Evans JD, and Jack JJ. Solutions for transients in arbitrarily branching cables:  
1096 II. Voltage clamp theory. *Biophys J* 65: 450-468, 1993b.

1097 Nadim F, and Golowasch J. Signal transmission between gap-junctionally coupled  
1098 passive cables is most effective at an optimal diameter. *J Neurophysiol* 95: 3831-3843,  
1099 2006.

1100 Nadim F, Olsen OH, De Schutter E, and Calabrese RL. Modeling the leech heartbeat  
1101 elemental oscillator. I. Interactions of intrinsic and synaptic currents. *J Comput*  
1102 *Neurosci* 2: 215-235, 1995.

1103 Neher E, and Marty A. Discrete changes of cell membrane capacitance observed under  
1104 conditions of enhanced secretion in bovine adrenal chromaffin cells. *Proc Natl Acad*  
1105 *Sci U S A* 79: 6712-6716, 1982.

1106 Pineda RH, Knoeckel CS, Taylor AD, Estrada-Bernal A, and Ribera AB. Kv1 potassium  
1107 channel complexes in vivo require Kvbeta2 subunits in dorsal spinal neurons. *J*  
1108 *Neurophysiol* 100: 2125-2136, 2008.

1109 Prinz AA, and Fromherz P. Effect of neuritic cables on conductance estimates for remote  
1110 electrical synapses. *J Neurophysiol* 89: 2215-2224, 2003.

1111 Puil E, Gimbarzevsky B, and Miura RM. Quantification of membrane properties of  
1112 trigeminal root ganglion neurons in guinea pigs. *J Neurophysiol* 55: 995-1016, 1986.

1113 Rabbah P, Golowasch J, and Nadim F. Effect of electrical coupling on ionic current and  
1114 synaptic potential measurements. *J Neurophysiol* 94: 519-530, 2005.

1115 Rall W. Core conductor theory and cable properties of neurons. In: *Handbook of*  
1116 *Physiology (Section 1, The Nervous System I, Cellular Biology of Neurons)*, edited by  
1117 Kandel ER. Bethesda, MD: American Physiological Society, 1977, p. 39-97.

1118 Royeck M, Horstmann MT, Remy S, Reitze M, Yaari Y, and Beck H. Role of axonal  
1119 NaV1.6 sodium channels in action potential initiation of CA1 pyramidal neurons. *J*  
1120 *Neurophysiol* 100: 2361-2380, 2008.

1121 Selverston AI, Russell DF, and Miller JP. The stomatogastric nervous system: structure  
1122 and function of a small neural network. *Prog Neurobiol* 7: 215-290, 1976.

1123 Siebert W. *Circuits, Signals, and Systems*. Cambridge: MIT Press, 1986.

1124 Solsona C, Innocenti B, and Fernandez JM. Regulation of exocytotic fusion by cell  
1125 inflation. *Biophys J* 74: 1061-1073, 1998.

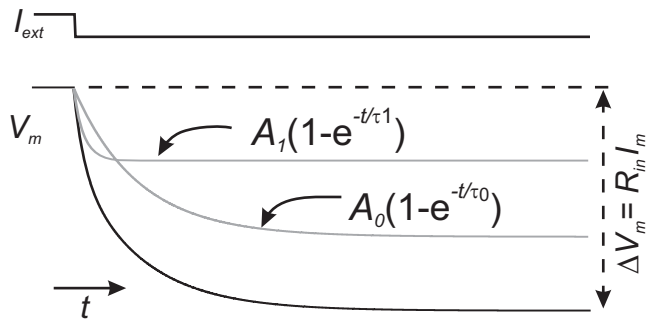
1126 Soto-Trevino C, Rabbah P, Marder E, and Nadim F. Computational model of electrically  
1127 coupled, intrinsically distinct pacemaker neurons. *J Neurophysiol* 94: 590-604, 2005.

1128 Spruston N, Jaffe DB, Williams SH, and Johnston D. Voltage- and space-clamp errors  
1129 associated with the measurement of electrotonically remote synaptic events. *J*  
1130 *Neurophysiol* 70: 781-802, 1993.

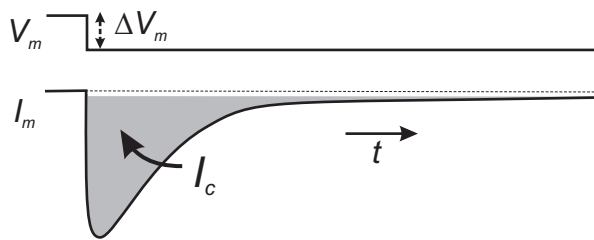
1131

1132

### A CC\_step



### B VC\_step



### C VC\_ramp

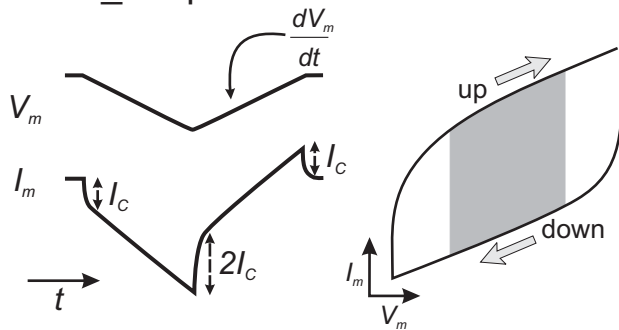


Figure 1  
Golowasch et al

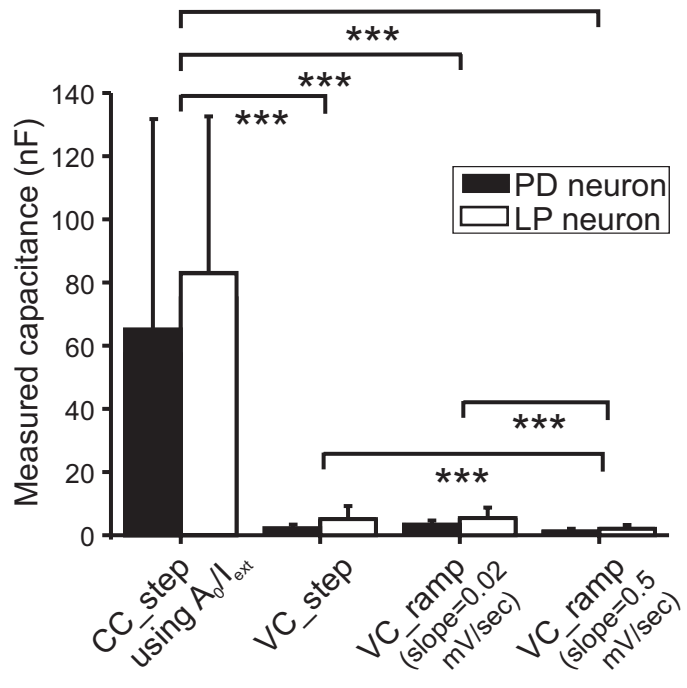


Figure 2  
Golowasch et al

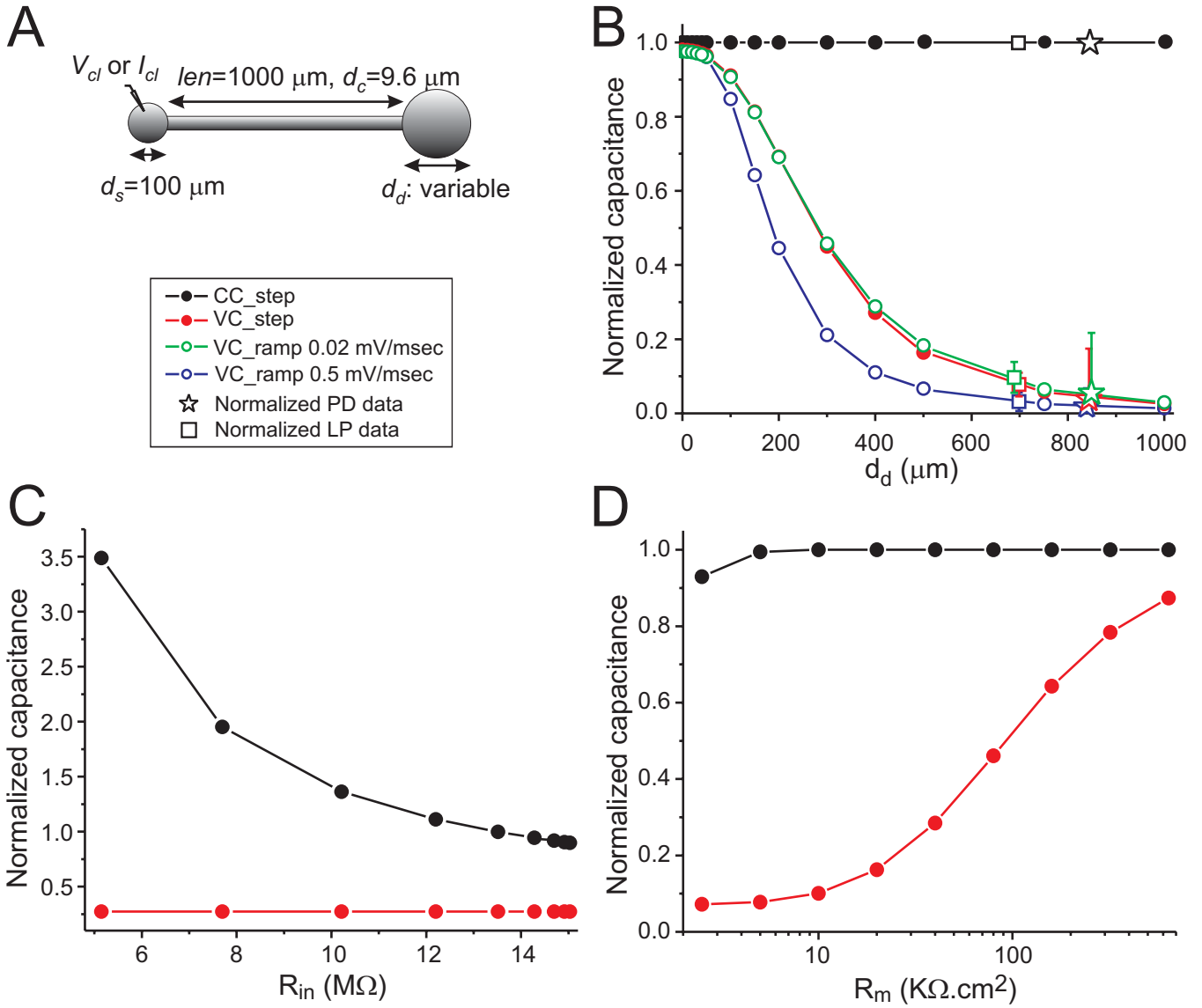


Figure 3  
 Golowasch et al

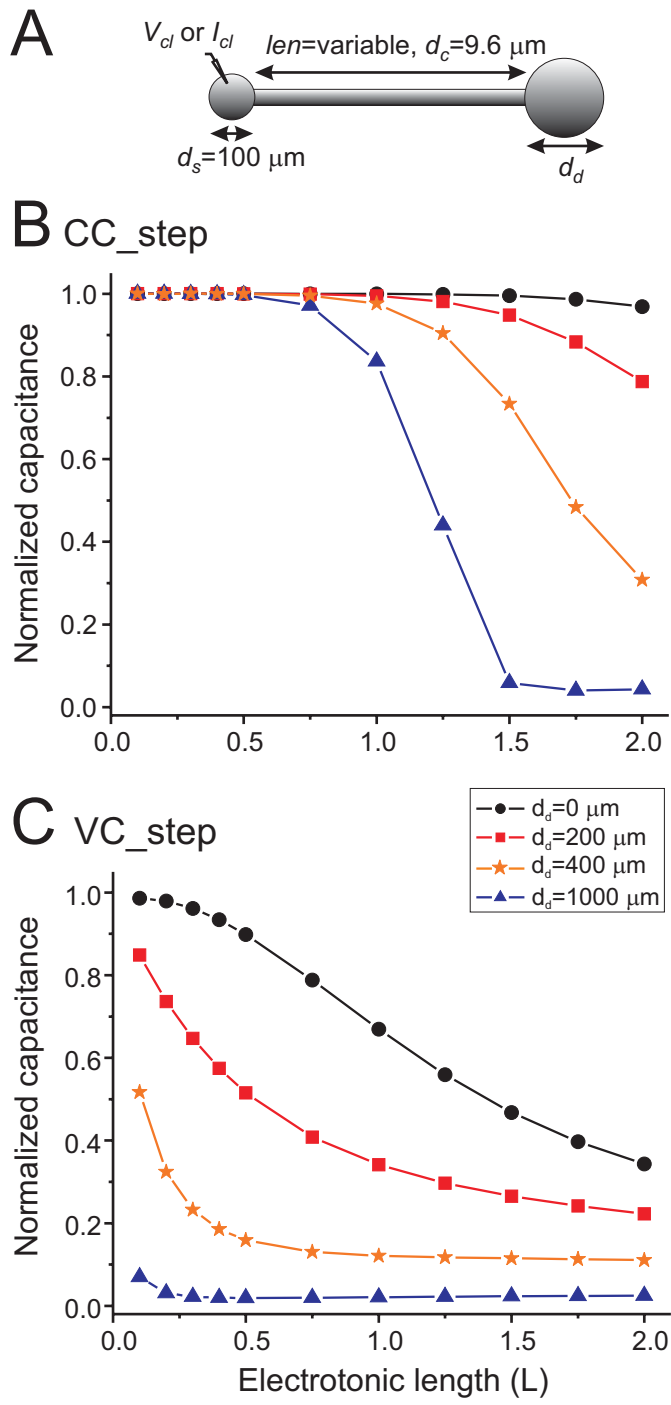
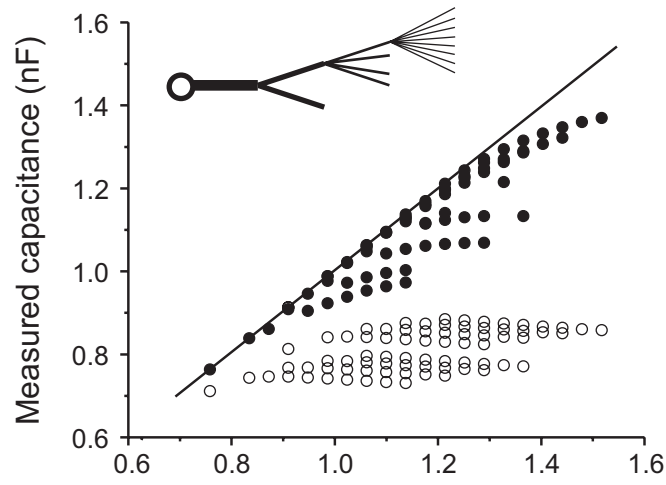
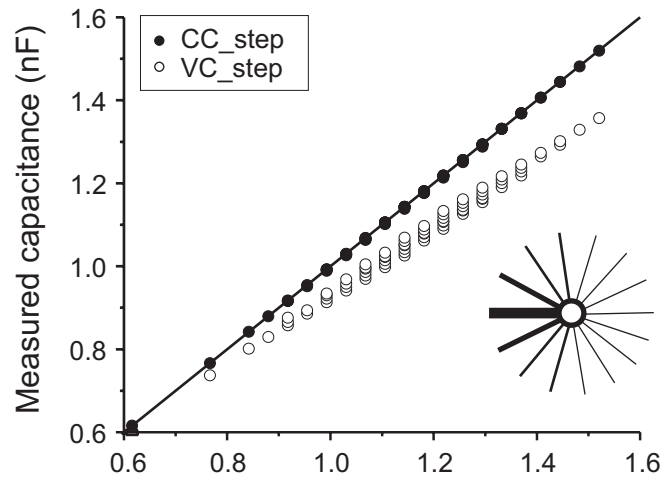


Figure 4  
 Golowasch et al

# A Asymmetric tree



# B Concentric



# C Symmetric tree

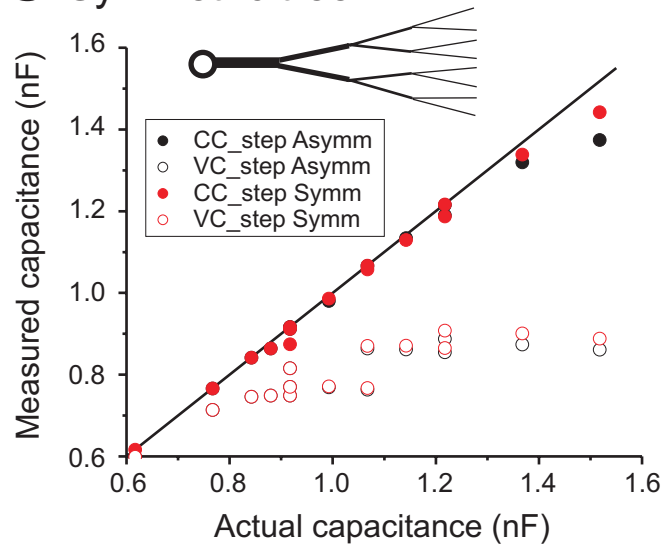


Figure 5  
Golowasch et al

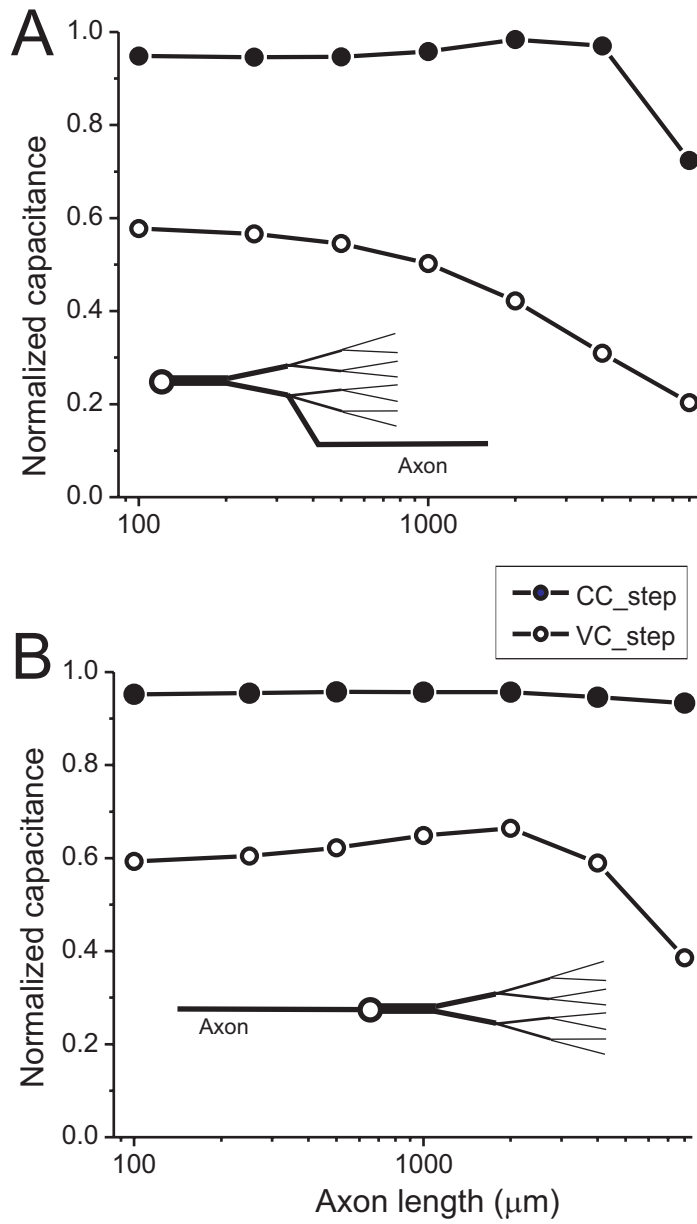
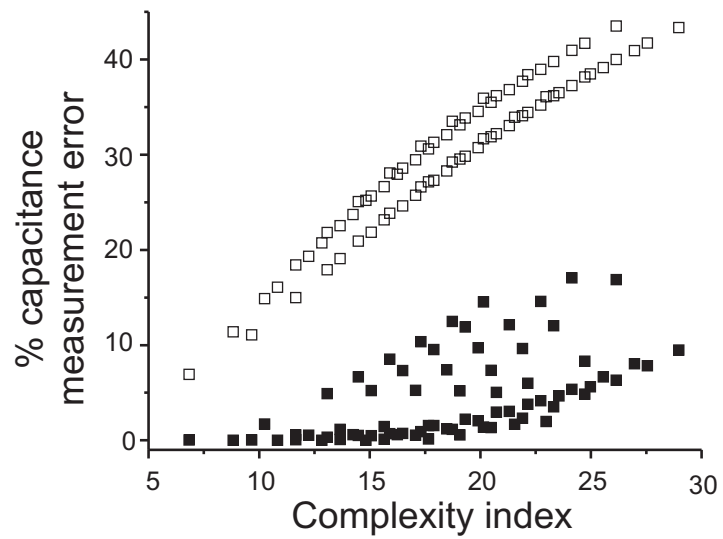


Figure 6  
Golowasch et al

### A Asymmetric tree



### B Concentric

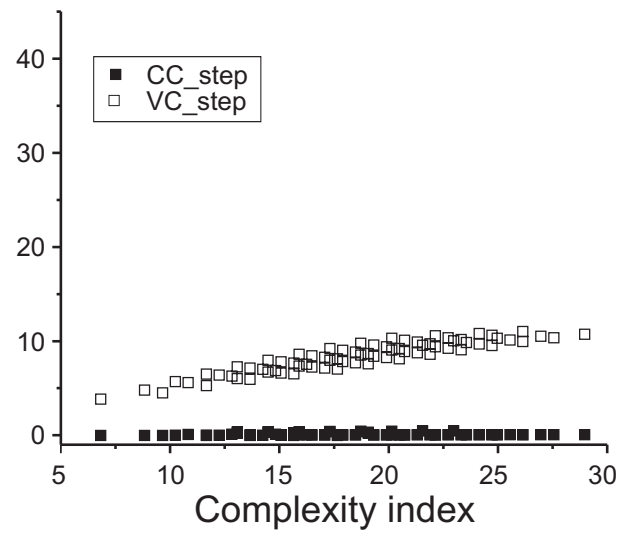


Figure 7  
Golowasch et al

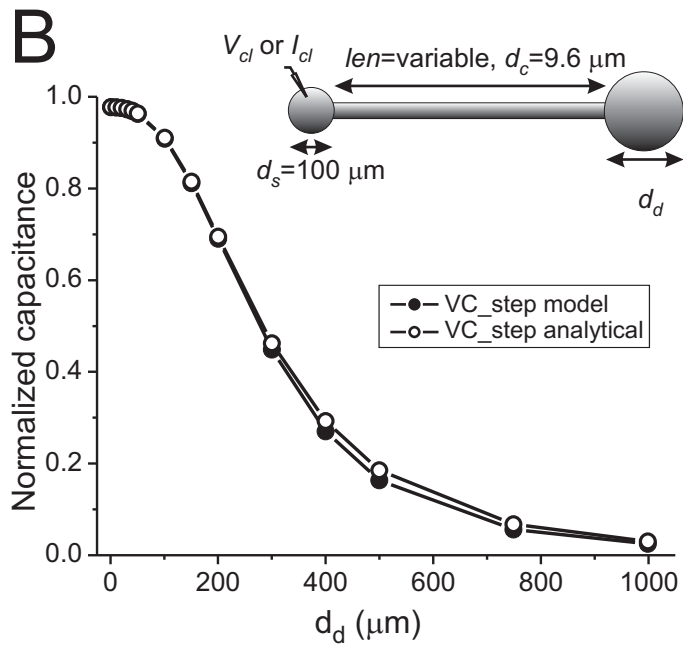
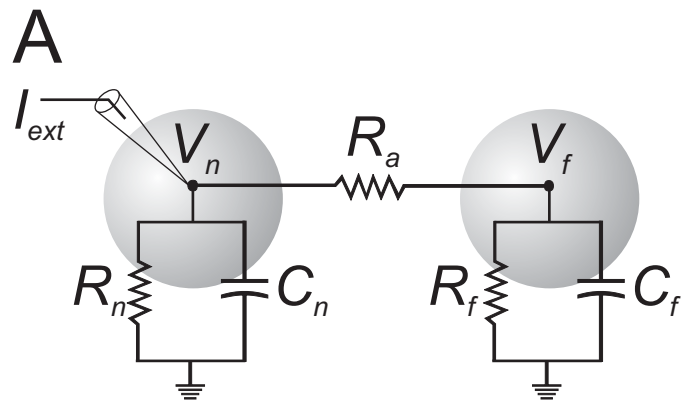


Figure 8  
Golowasch et al